Disentangling The Causes of Discrepancies In Simulated Immersion-mode Ice Nucleating Particles

Aishwarya Raman[1], Elise K Wilbourn[2], Mikhail S. Pekour[3], Naruki Hiranuma[4], and Susannah Marie Burrows[3]

[1]Pacific Northwest National Laboratory
[2]Sandia National Laboratory
[3]Pacific Northwest National Laboratory (DOE)
[4]West Texas A&M University

March 26, 2023

Abstract

We assess the predictability of immersion-mode ice nucleating particles (INPs) at a remote marine site in the Eastern North Atlantic (ENA) using aerosol simulations from a global climate model as inputs to the immersion-mode INP parameterizations. While the model- simulated INP concentrations are lower by one to three orders of magnitudes compared to the measurements, we achieve aerosol-INP closure at ENA using the observed aerosol properties. We demonstrate a novel INP error decomposition approach to quantify the portion of total INP error from different error components. We conclude that inaccuracies in aerosols (surface area and composition) are the dominant cause of the model INP discrepancy at ENA. We recommend that, for future aerosol-INP closure studies, along with the measurements for total INP concentrations, campaigns should also collect co-located aerosol size-resolved composition measurements (in the INP-relevant size range) to better distinguish and quantify the error sources.

Disentangling The Causes of Discrepancies In Simulated Immersion-mode Ice Nucleating Particles

Aishwarya Raman [1], Elise K. Wilbourn [2,3], Mikhail S. Pekour[1], Naruki Hiranuma [2], Susannah M. Burrows[1]

[1]Pacific Northwest National Lab, Richland, WA
[2]Dept. of Life, Earth and Environmental Sciences, West Texas A&M University,Canyon, TX
[3]*Now at Sandia National Laboratories,Livermore, CA

Key Points:

- Global climate model simulated immersion-mode INP concentrations are one to three orders of magnitude lower than INP measurements.
- Aerosol-INP closure is achieved (INPs within a factor of 10) for INPs simulated using the in situ aerosol measurements
- Errors in the model-simulated aerosol properties are the dominant cause of the model INP discrepancy .

Abstract

We assess the predictability of immersion-mode ice nucleating particles (INPs) at a remote marine site in the Eastern North Atlantic (ENA) using aerosol simulations from a global climate model as inputs to the immersion-mode INP parameterizations. While the model-simulated INP concentrations are lower by one to three orders of magnitudes compared to the measurements, we achieve aerosol-INP closure at ENA using the observed aerosol properties. We demonstrate a novel INP error decomposition approach to quantify the portion of total INP error from different error components. We conclude that inaccuracies in aerosols (surface area and composition) are the dominant cause of the model INP discrepancy at ENA. We recommend that, for future aerosol-INP closure studies, along with the measurements for total INP concentrations, campaigns should also collect co-located aerosol size-resolved composition measurements (in the INP-relevant size range) to better distinguish and quantify the error sources.

Plain Language Summary

We assess the predictability of ice nucleating particles (INPs) at a remote marine site in the Eastern North Atlantic (ENA) using aerosol simulations from a global climate model as inputs to the immersion-mode INP parameterizations. Model-simulated INP concentrations at ENA are lower by one to three orders of magnitude compared to the measurements. However, INPs predicted using the observed aerosol properties are within an order of magnitude from INP measurements. We quantify the portion of errors from aerosol and INP parameterization components. We conclude that inaccuracies in aerosol surface area and composition are the dominant causes for the model INP discrepancy at ENA.

1 Introduction

Mixed-phase clouds (MPCs) play a vital role in precipitation and radiation budget due to the presence of super-cooled liquid water and ice crystals (Korolev et al., 2017; Burrows et al., 2022). The dominant mechanism for heterogeneous ice formation in MPCs is the immersion-mode freezing of cloud droplets in the presence of ice nucleating particles (INPs) at temperatures warmer than $-38\,^{\circ}\mathrm{C}$ (Pruppacher et al., 1998; Vali et al., 2015). INPs are a rare subset of aerosols whose ice nucleating ability depends on the size-resolved particle composition, abundance, surface properties, and atmospheric conditions (e.g. DeMott et al., 2010; Boose et al., 2016).

In general, the INP number concentrations in the marine atmosphere are lower by an order of magnitude or more compared to those in terrestrial regions (e.g. DeMott et al., 2016). However, sea spray (salt + organics) emitted from bubble bursting in the ocean and mineral dust transported to the marine atmosphere from deserts can significantly affect the INP population in the marine boundary layer (e.g. Creamean et al., 2019; McCluskey et al., 2019). Previous studies over remote marine regions have shown that presence of INPs can alter climate feedbacks (e.g. Vergara-Temprado et al., 2018; Tan et al., 2022), but climate models can exhibit significant bias in prediction of INPs (Raman et al., 2022).

The predictive understanding of INPs in climate models is limited by sparse measurements of co-located aerosol size-resolved composition and INP number concentration. Recent INP studies have resorted to aerosol-INP closure experiments to investigate the error sources in INP prediction. Aerosol-INP closure for a given INP measurement temperature is defined as the agreement between the predicted INPs from observed aerosol properties and the measured INP concentrations within measurement uncertainties (Burrows et al., 2022). Knopf et al. (2021) conducted aerosol-INP closure during a frontal passage at the Department of Energy (DOE) site in the Southern Great Plains, and found that size-resolved INP com-

position and individual INP propensity are especially important for closure in regions with frequent variations in meteorological and aerosol conditions.

In this study, we assess the dominant cause of errors in the boundary-layer immersion-mode INP predictability during the DOE field campaign, Examining the Ice Nucleating Particles from the Eastern North Atlantic (ExINP-ENA), from October 2020 to December 2020 (Hiranuma et al., 2022). We perform aerosol-INP closure at ENA (39.09°N, 28.02°W) (Text S1) and constrain the spread in modeled INP concentrations using different aerosol measurements and INP parameterizations. We introduce a novel error decomposition approach to quantify the portion of total INP discrepancy between model and observations associated with individual error sources. We illustrate the methods for the aerosol-INP closure and INP error decomposition in Section 2, describe and discuss our findings in Section 3 and Section 4.

2 Methods

2.1 Aerosol and INP Measurements

We summarize the suite of aerosol and INP measurements in Table S1. We estimate the total aerosol surface area per unit volume (S_{aer} [$m^2\,m^{-3}$]) and related uncertainties using the ARM Aerosol Observing System (AOS) nephelometer-based aerosol scattering efficiency measurements (DeMott et al., 2016; Testa et al., 2021) at 450 nm wavelength (Text S3). We calculate six hourly averages of S_{aer} estimates to match time stamps in the INP measurements. For particle-type classification, we use the elemental composition data (based on 100 particle samples) from scanning electron microscopy coupled with energy-dispersive X-ray spectroscopy (SEM-EDX) (China et al., 2017). We estimate the total atomic weight proportion for dust and sea spray particles using the classification techniques in Cheng et al. (2016) and Hiranuma et al. (2013) (Text S4 and Table S2).

We use immersion mode ambient INP number concentrations measured with the Portable Ice Nucleation Experiment (PINE) chamber (Bilfinger Noel, model PINE-3) (Möhler et al., 2021) at temperatures between $-14\,°C$ and $-33\,°C$. INP concentrations were measured approximately every 12 minutes, and measurements were averaged for six hours to obtain adequate sampling statistics in a clean marine environment. We derive temperature-dependent errors for INP concentrations (Hiranuma et al., 2022) in terms of a 95% confidence interval (CI) using the Poisson statistics (Krishnamoorthy & Lee, 2013) (Text S6).

2.2 Model Overview and INP Parameterizations

We use the U.S. DOE Energy Exascale Earth System Atmosphere Model version 1 (EAMv1) (Neale et al., 2010; Golaz et al., 2022) with the modal aerosol module with four log-normal modes (MAM4) (H. Wang et al., 2020) to simulate the size-resolved aerosol composition inputs for the INP parameterizations. We provide more details about the EAMv1 model in Text S7.

We quantify the IN efficiency ($n_s(T)$ [INP concentrations per unit area, m^{-2}]) for dust and sea spray INPs using the temperature-dependent ice nucleation active site (INAS) parameterizations (Table S3). We derive INP concentrations by multiplying the $n_s(T)$ estimates with dust/sea spray surface area, depending on the INP type.

We include only dust and sea spray INPs at ENA because these two aerosol types have been commonly observed at ENA in previous studies (Y. Wang et al., 2020; Zheng et al., 2018). We estimate sea spray $n_s(T)$ following McCluskey et al. (2018). For dust INPs, we use multiple $n_s(T)$ parameterizations: Boose et al. (2016) (B16 Morocco, B16 Pelopennese),

Ullrich et al. (2017) (UL17), and Reicher et al. (2019) (REI19 super-micron) (Text S8 and Text S9).

2.3 Experiment Design and INP Closure

We ran EAMv1 simulations for the period of January-December 2020 with approximately 100 km horizontal resolution and 72 vertical layers using prescribed sea surface temperature and constrained meteorology (S. Zhang et al., 2022). We nudged the model winds at all model vertical levels using the Modern-Era Retrospective Analysis for Research and Applications, version 2 (MERRA-2) reanalysis data (Gelaro et al., 2017) at a 6-h relaxation time scale.

To permit spatial and temporal co-location between model outputs and INP measurements, we use the simulated aerosol fields at the nearest model grid box to the ENA station and use the 6-hourly averaged model outputs to estimate INP concentrations. We calculate the INP concentrations offline (i.e. model cloud microphysics is not affected by the INPs simulated in this study) by using the EAMv1-simulated and co-located dust and sea spray aerosols and the INP parameterizations.

We characterize the INP discrepancy between EAMv1-predicted INPs and PINE measurements in terms of modified normalized bias (MNB) (Equation 1), which is calculated as the difference in two quantities divided by the sum of the quantities (Text S10). Equation 1 shows a general formula for estimating MNB from two INP calculations, $\mathrm{INP}_1(T)$ and $\mathrm{INP}_2(T)$.

$$\mathrm{MNB}\left(\mathrm{INP}_1(T), \mathrm{INP}_2(T)\right) = \frac{\mathrm{INP}_1(T) - \mathrm{INP}_2(T)}{\mathrm{INP}_1(T) + \mathrm{INP}_2(T)}\,. \tag{1}$$

To quantify the aerosol-INP closure (schema in Figure S3), we estimate INP concentrations using the observed aerosol properties ('closure INPs'), nephelometer-estimated S_{aer} and the SEM-EDX derived fraction of dust and sea spray in the total chemical composition for 100 SEM-EDX samples. We declare aerosol-INP closure if the closure INP estimates are within a factor of 10 from the measurements. We express the closure error using the MNB metric.

Several climate modeling studies in the literature have adopted error decomposition techniques to determine the dominant processes contributing to bias in GCM simulated feedbacks (e.g. Tian et al., 2009; Y. Zhang et al., 2021; Zelinka et al., 2016). For a given INP measurement temperature, we express the total predicted INP discrepancy (E_p) as a linear combination of three error sources: the portion of E_p associated with S_{aer} ($E_{S_{aer}}$), composition (E_c), and residual sources (E_{res}) (Equation 2). Finally, we quantify the uncertainty in each error source given the independent aerosol and INP measurements, each with an uncertainty (Table 2). We use an uncertainty propagation technique to quantify the uncertainties in E_c and E_{res} (Text S11).

$$E_{\mathrm{p}} = E_{\mathrm{Saer}} + E_{\mathrm{c}} + E_{\mathrm{res}}\,. \tag{2}$$

3 Results

3.1 Comparing Simulated and Observed Aerosol Properties

Figure 1 compares the co-located surface level dust (Figure 1a), sea spray (Figure 1b), and total surface area (Figure 1c) from EAMv1 simulations and in situ measurements at ENA.

Experiment name	**Surface area**	**Aerosol composition**
INP E3SM	S_{aer} from E3SM for the size range $0.08 - 10\mu m$	E3SMv1 simulations of dust and sea spray aerosol fractions
INP E3SM NEPH	Dust and sea spray aerosol surface were calculated using S_{aer} from the AOS nephelometer	E3SMv1 simulations of dust and sea spray aerosol fractions
INP EDX E3SM	S_{aer} from E3SMv1	Aerosol fraction for dust and sea spray from SEM-EDX
INP EDX NEPH	S_{aer} from the nephelometer	Aerosol fraction for dust and sea spray from SEM-EDX

Table 1. INP calculations using various observed and simulated aerosol quantities.

Overall, the EAMv1-simulated surface area estimates are typically lower by one to two orders of magnitude compared to the in situ measurements. For the particle-type fraction, EAMv1 overestimates sea spray fraction and underestimates dust fraction compared to SEM-EDX measurements, both approximately by an order of magnitude. To better understand the aerosol classification at ENA, we compare our SEM-EDX classification with Knopf et al., 2022 analysis at the ENA site (Text S5).

The biases in EAMv1-simulated aerosols over the remote marine regions are mainly due to the high vertical resolution and higher dry deposition rates in the model (a factor of two compared to CAM5 and other AeroCom (Aerosol Comparisons Observations and Models) models) (Wu et al., 2020; Feng et al., 2022). Such biases in dry deposition velocities are not uncommon to global models (e.g. Emerson et al., 2020). In addition to dry deposition, aerosol biases in EAMv1 are also affected by biases in other physical processes such as aerosol wet scavenging (K. Zhang et al., 2022). In marine regions where INP concentrations are already lower compared to continental regions, systematic differences between the simulated and observed aerosol surface area and composition as large as two orders of magnitude will directly affect the magnitude of INPs estimated using the simulated aerosol quantities.

3.2 INP Concentrations at ENA

Figure 2 compares the 6-hourly averaged INP number concentration measurements from PINE with EAMv1-simulated (and co-located) dust and sea spray INP concentrations for different measurement temperatures. The lack of strong seasonal variability in the INP measurements at ENA suggests that dust and sea spray INPs are persistent INP sources throughout the year. The INP number concentration measurements over the study period range from $0.1\,\mathrm{L}^{-1}$ to $100\,\mathrm{L}^{-1}$ for temperatures between $-20\,^{\circ}\mathrm{C}$ and $-30\,^{\circ}\mathrm{C}$ respectively. However, INP E3SM estimates (Blue lines in Figure 2) are generally lower by one to two orders of magnitudes compared to the INP measurements. We find that combining EAMv1-simulated sea spray (M18) and dust INPs provides little improvement in the model-observation discrepancy at ENA.

Among the dust INP parameterizations (Table S3), UL17, B16 Pelopennese, and B16 Morocco show the maximum, median, and minimum discrepancies with measurements, respectively. Higher INP concentrations in B16 Morocco are likely due to the higher IN propensity of milled dust samples used for the development of the parameterization (Boose et al., 2016). Milling increases the surface irregularities, which in turn increases the IN activity (Reicher et al., 2019). Given these caveats about the IN efficiency of milled dust samples, it is possible that the good agreement between simulated B16 Morocco INPs and PINE measurements at ENA is likely due to the compensating errors between dust surface area underestimation in EAMv1 and $n_s(T)$ overestimation in B16 Morocco.

Error source / Calculation	**Purpose**	**Uncertainty calculation**
$E_p = \mathrm{MNB}(\mathrm{INP}_{\mathrm{E3SM}}, \mathrm{INP}_{\mathrm{OBS}})$	Total predictive skill error for E3SM v1 simulated vs. observed INP concentrations	Associated with different dust INP parameterizations.
$E_{S_{\mathrm{aer}}} = \mathrm{MNB}(\mathrm{INP}_{\mathrm{E3SM}}, \mathrm{INP}_{\mathrm{E3SM\ NEPH}})$	Portion of E_p associated with mismatch in simulated and observed S_{aer}	Calculated using uncertainties in the nephelometer scattering coefficients, Q (lower bound = 0.42, upper bound = 3.0).
$E_{\mathrm{c}} = \mathrm{MNB}(\mathrm{INP}_{\mathrm{E3SM\ NEPH}}, \mathrm{INP}_{\mathrm{EDX\ NEPH}})$	Portion of $E_{S_{aer}}$ associated with mismatch in E3SMv1 simulated vs. observed aerosol composition.	Calculated by propagating standard errors in SEM-EDX aerosol fraction to MNMB. For E3SM NEPH, we use a median Q = 2.0.
$E_{\mathrm{res}} = \mathrm{MNB}(\mathrm{INP}_{\mathrm{EDX\ NEPH}}, \mathrm{INP}_{\mathrm{OBS}})$	Residual errors (e.g., missing INP sources, errors in INP parameterizations, and atmospheric transformation of INPs.)	Calculated by propagating temperature dependent errors in measurements to MNMB. We use a median dust and sea spray fraction from EDX.

Table 2. INP error decomposition and uncertainty calculation for individual error components

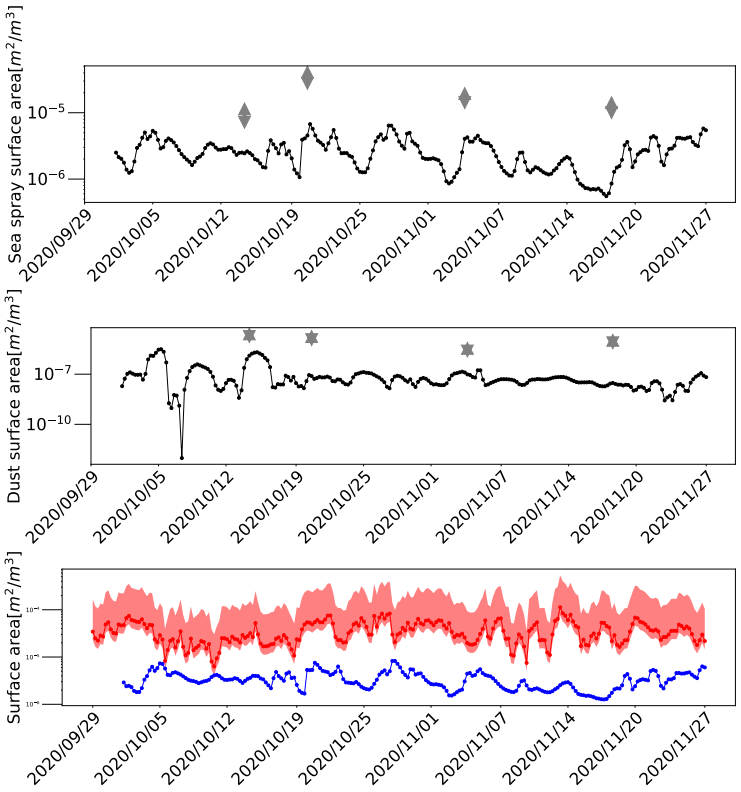

Figure 1. (a) Simulated (black) and observed (grey) dust surface area from E3SMv1 simulations and SEM-EDX (dust fraction) + Nephelometer (total surface area), respectively, along with the measurement uncertainties. (b) Same as (a) but comparing observations and model for sea spray aerosol surface area. (c) Simulated (blue) and observed (red) total surface area from E3SMv1 and the Nephelometer, respectively, along with the Nephelometer surface area uncertainties (red shaded region) calculated using the upper (3.0) and lower (0.42) bound for assumptions of scattering coefficients. Surface area estimates shown here for EAMv1 cover the size range 80 nm to 10 µm. In panels (a) and (b), observed surface area for dust and sea spray was estimated using the SEM-EDX particle-type classification. Each SEM-EDX measurement represents a sampling period of two to three days. To calculate the dust and sea spray surface area using the SEM-EDX particle-type classification data, we used the total surface area from the Nephelometer corresponding to the last day of the SEM-EDX measurement.

Overall, the uncertainty in the model discrepancies for different INP parameterizations is in the same order of magnitude as the discrepancy due to the simulated aerosol properties (Figure 2, blue and red lines). This leads to the next question, what is the dominant cause of the model INP discrepancies at ENA - aerosol errors or deficiencies in the INP parameterizations?

3.3 INP Closure, Error Decomposition, and Uncertainty Propagation

Figure 2 compares the closure INPs (green squares) predicted using the observed aerosol properties against the EAMv1-simulated (blue) and measured (black) INP concentrations. We find that adding sea spray and dust INPs does not reduce the closure. The closure INPs (Figure 2, green squares) are within an order of magnitude from the PINE measurements, the criterion we use in this study for aerosol-INP closure. These results confirm that the

[ht]

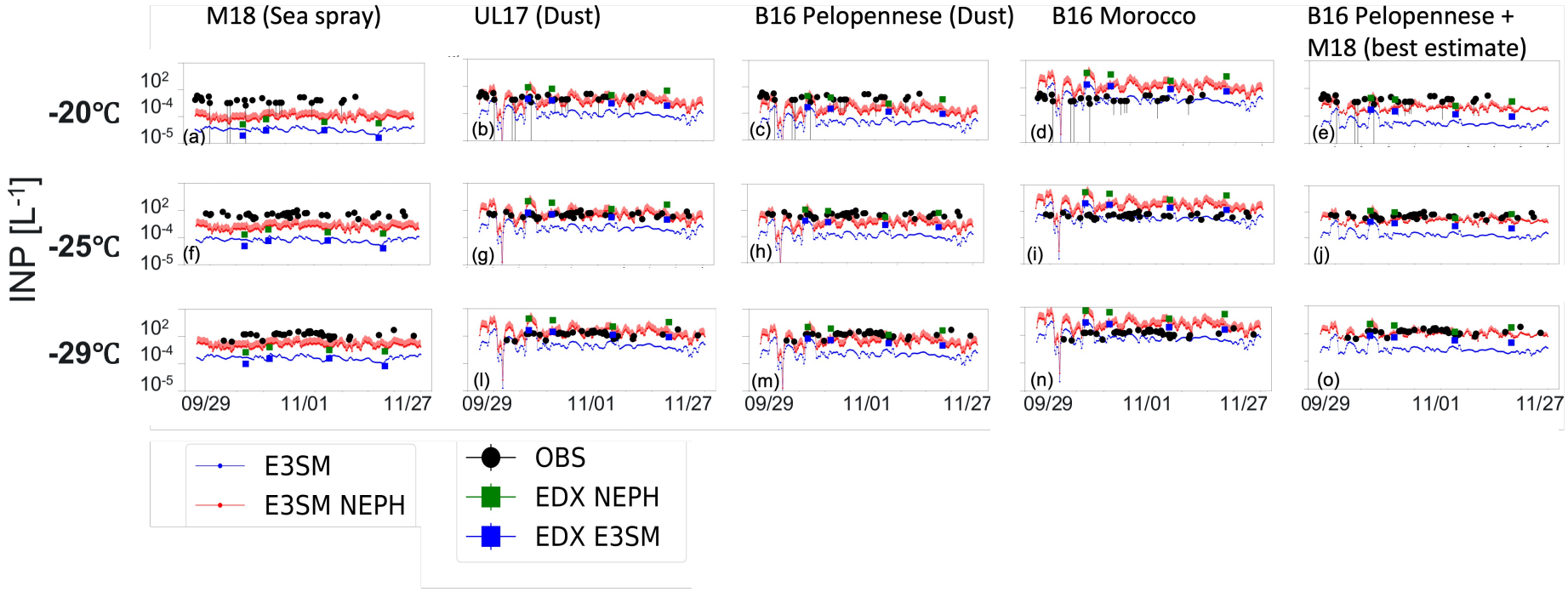

Figure 2. Time series of observed and modeled INP concentrations at −20°C,−25°C and −29°C. INP concentrations from PINE observations (ENA OBS) are shown as black circles. Different INP calculations are listed in Table 1.

EAMv1-simulated INP discrepancies as high as two to three orders of magnitude cannot be explained only by the deficiencies in the INP parameterizations.

Figure 3 illustrates the decomposition of model INP discrepancies (E_p) into error components associated with the simulated surface area ($E_{S_{aer}}$), composition (E_c), and the residual sources (closure error) (E_{res}). We find that $E_{S_{aer}}$+ E_c together estimate 20-30% higher median MNB compared to the MNB for E_{res}. The opposite signs for E_{res} and aerosol components ($E_{S_{aer}}$ and E_c) indicate that these two error sources partially compensate for one another. Therefore, improving only the INP parameterization errors without improving the aerosol errors in the model simulations will result in compensating biases in the model-predicted INPs.

We conclude that the inaccuracies in aerosol surface area and composition simulated in EAMv1 are the major reasons for the large discrepancy in model-predicted INP concentrations during the ExINP-ENA campaign. Along with improving the representation of aerosol properties in the model, accounting for deficiencies in the INP parameterizations by including missing INP sources and INP chemistry (e.g. biological INPs, coating of dust by sulfuric acid (Huang et al., 2021; Sullivan et al., 2010)) can further improve the INP closure at ENA.

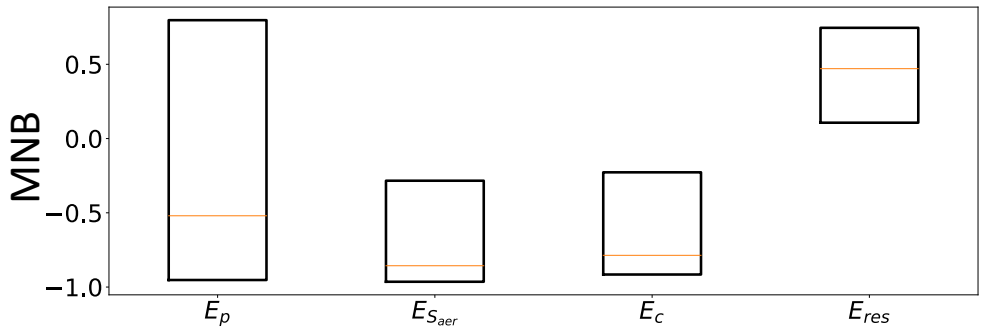

Figure 3. Decomposition of total INP discrepancies (dust and sea spray) at −29°C into individual error components, $E_{S_{aer}}$, E_c, and E_{res}. Table 2 describes the error components and uncertainties. The uncertainties in E_p are from using different dust INP parameterizations. For other error components, we show results only for the B16 Peloponnese + M18 INPs which have the least closure error compared to other dust parameterizations. Different nephelometer surface area estimates are derived based on the uncertainties in the scattering coefficient assumptions. The MNB range in $E_{S_{aer}}$ corresponds to using the lower and upper bound for nephelometer-derived surface area estimates in the INP parameterizations. Due to the limited number of temporally coincident observations from EDX, Neph, and PINE, sampling days for error sources are not the same. The number of days used for the calculation of E_p and $E_{S_{aer}}$ and their associated uncertainties are: 238 and 226. E_c and E_{res} represent four coincident SEM-EDX and INP samples. Upper and lower bounds for E_c are calculated using the variability in EDX errors in dust and sea spray fractions for different days during the campaign. We calculate E_{res} only for −29°C because of the limited availability of coincident measurements for SEM-EDX particle-type classification, PINE INP measurements, and temperature-dependent INP measurement errors at this temperature.

4 Discussion and Conclusion

In this study, we have investigated the predictive capability of EAMv1 and INAS-based INP parameterizations to simulate immersion-mode INP concentrations during the ExINPENA campaign at ENA, with an eye towards determining the leading cause of model-observation INP discrepancies. The EAMv1-simulated INP concentrations are one to three orders of magnitude lower than the INP measurements from PINE. We achieve INP closure (INP discrepancy within a factor of 10) when INPs are predicted using the measured aerosol properties from the AOS nephelometer and SEM-EDX. This evidence confirms that we cannot reduce such large discrepancies in the predicted INPs only by resolving the flaws in the INP parameterizations, but it is important to accurately represent the aerosol properties in the model to improve INP predictions.

We have demonstrated a novel INP error decomposition to quantify the portion of total INP model-observation discrepancies from different error sources. At the ENA site, we find that the inaccuracy in the EAMv1-simulated aerosol properties is the leading cause for the model INP discrepancies. Therefore, we conclude that correctly simulating the aerosol physical and chemical processes in the model is critical for accurately predicting the immersion-mode INP concentrations at ENA.

We note below some caveats of this study and their implications for the results. We used EAMv1-simulated aerosols for particle size range from 80 nm to 10 µm, whereas, PINE INP measurements are sensitive only up to 3 µm. Additionally, SEM-EDX size distribution data for ENA (for 100 samples) showed that only 10 to 17% of the surface area is between 3 µm and 5 µm. Therefore, almost an order of magnitude difference between the observed and simulated INPs cannot be attributed predominantly to the differences in the size cut off between PINE and the nephelometer.

We demonstrated the INP error decomposition method only for $-29\,^{\circ}\mathrm{C}$, because we did not have co-located SEM-EDX and INP measurements for other temperatures. Although we have considered only the temperature-dependent errors associated with counting statistics in the closure calculations, we recognize that other systematic uncertainties (e.g. loss of larger ice crystals between the PINE chamber and the optical counter, overlap in the size distribution of smaller ice crystals with the larger particles not activated to droplets) can also affect the INP measurements. Möhler et al. (2021) showed that for immersion freezing of mineral dust aerosols, PINE INP measurements were within the experimental uncertainties (%20) of the INP measurements from the Aerosol Interaction and Dynamics in the Atmosphere cloud chamber experiments.

Despite these caveats, this study provides key insights into the dominant sources of errors in immersion-mode INPs in the EAMv1 climate model. The INP error decomposition method we have demonstrated here can be modified and applied to other regions and field experiments. The information gained from the decomposition enables us to make recommendations for both model development and future field campaigns.

Improving INPs in climate models can significantly impact the simulated super-cooled liquid water (SLW) in MPC clouds, albedo, and climate. For example, a global climate modeling study found that with fewer INPs, the negative cloud-phase feedback was weakened, and strongly impacting the sea ice loss and Arctic Amplication (Tan et al., 2022). Overall, by better diagnosing and reducing the causes of INP errors, we can improve confidence in the use of aerosol-aware INP parameterizations in climate models and consequently reduce uncertainites in climate predictions (Burrows et al., 2022).

Acknowledgments

A. Raman thanks Catherine L. Himes from the PNNL communication team for technical editing support. A. Raman and S.M. Burrows were funded by the U.S. Department of Energy (DOE), Office of Science, Office of Biological and Environmental Research through the Early Career Research Program. N.Hiranuma and E.K.Wilbourn were funded under the DOE grant DE-SC-0018979. The Pacific Northwest National Laboratory is operated for DOE by Battelle Memorial Institute under contract DE-1713 AC05-76RL01830. E. K. Wilbourn and High-performance computing resources for this project was provided by the PNNL Research Computing, and the National Energy Research Scientific Computing Center (NERSC), a DOE Office of Science User Facility supported by the Office of Science of the U.S. Department of Energy under Contract No. DE-AC02-05CH11231.

Data Availability Statement E3SMv1 model simulated and co-located aerosol and INP data at ENA, SEM-EDX observations, nephelometer-based surface area estimates, and the corresponding Python scripts used for the analysis are available in the Zenodo repository DOI:10.5281/zenodo.7746607. PINE INP observations are archived in the ARM repository `https://www.arm.gov/research/campaigns/ena2020exinpena`. Aerosol scattering measurements from the Nephelometer are available in the ARM archive `https://adc.arm.gov/discovery/#/results/s::nephelometer`

Supporting Information ENAGRLSIworking.pdf

References

Boose, Y., Welti, A., Atkinson, J., Ramelli, F., Danielczok, A., Bingemer, H. G., ... Lohmann, U. (2016). Heterogeneous ice nucleation on dust particles sourced from nine deserts worldwide–part 1: Immersion freezing. *Atmospheric Chemistry and Physics*, *16*(23), 15075–15095.

Burrows, S. M., McCluskey, C. S., Cornwell, G., Steinke, I., Zhang, Kai, ... others (2022). Ice-nucleating particles that impact clouds and climate: Observational and modeling research needs. *Reviews of Geophysics*, e2021RG000745.

Cheng, C.-L., Chang, H.-H., Chen, T.-H., Tsai, P.-J., Huang, Y.-T., Huang, P.-J., & Lin, S.-Y. (2016). Spectral and morphological classification of different chronic and acute taiwanese gallstones via ftir, sem and esem-edx microanalyses. *Digestive and Liver Disease*, *48*(5), 519–527.

China, S., Alpert, P. A., Zhang, B., Schum, S., Dzepina, K., Wright, K., ... others (2017). Ice cloud formation potential by free tropospheric particles from long-range transport over the northern atlantic ocean. *Journal of Geophysical Research: Atmospheres*, *122*(5), 3065–3079.

Creamean, J., Cross, J. N., Pickart, R., McRaven, L., Lin, P., Pacini, A., ... others (2019). Ice nucleating particles carried from below a phytoplankton bloom to the arctic atmosphere. *Geophysical Research Letters*, *46*(14), 8572–8581.

DeMott, P. J., Hill, T. C., McCluskey, C. S., Prather, K. A., Collins, D. B., Sullivan, R. C., ... others (2016). Sea spray aerosol as a unique source of ice nucleating particles. *Proceedings of the National Academy of Sciences*, *113*(21), 5797–5803.

DeMott, P. J., Prenni, A. J., Liu, X., Kreidenweis, S. M., Petters, M. D., Twohy, C. H., ... Rogers, D. (2010). Predicting global atmospheric ice nuclei distributions and their impacts on climate. *Proceedings of the National Academy of Sciences*, *107*(25), 11217–11222.

Emerson, E. W., Hodshire, A. L., DeBolt, H. M., Bilsback, K. R., Pierce, J. R., McMeeking, G. R., & Farmer, D. K. (2020). Revisiting particle dry deposition and its role in radiative effect estimates. *Proceedings of the National Academy of Sciences*, *117*(42), 26076–26082.

Feng, Y., Wang, H., Rasch, P., Zhang, K., Lin, W., Tang, Q., ... Yu, H. (2022). Global dust cycle and direct radiative effect in e3sm version 1: Impact of increasing model resolution. *Journal of Advances in Modeling Earth Systems*, *14*(7), e2021MS002909.

Gelaro, R., McCarty, W., Suárez, M. J., Todling, R., Molod, A., Takacs, L., ... others (2017). The modern-era retrospective analysis for research and applications, version 2 (merra-2). *Journal of climate*, *30*(14), 5419–5454.

Golaz, J.-C., Van Roekel, L. P., Zheng, X., Roberts, A. F., Wolfe, J. D., Lin, W., ... others (2022). The doe e3sm model version 2: overview of the physical model and initial model evaluation. *Journal of Advances in Modeling Earth Systems*, *14*(12).

Hiranuma, N., Brooks, S. D., Moffet, R. C., Glen, A., Laskin, A., Gilles, M. K., ... McFarquhar, G. (2013). Chemical characterization of individual particles and residuals of cloud droplets and ice crystals collected on board research aircraft in the isdac 2008 study. *Journal of Geophysical Research: Atmospheres*, *118*(12), 6564–6579.

Hiranuma, N., Wilbourn, E. K., & Lacher, L. (2022). *Examining the ice-nucleating particles from the eastern north atlantic (exinp-ena) field campaign report* (Tech. Rep.). Oak Ridge National Lab.(ORNL), Oak Ridge, TN (United States). Atmospheric ....

Huang, S., Hu, W., Chen, J., Wu, Z., Zhang, D., & Fu, P. (2021). Overview of biological ice nucleating particles in the atmosphere. *Environment International*, *146*, 106197.

Knopf, D. A., Barry, K., Brubaker, T., Jahl, L., Jankowski, K., Li, J., ... others (2021). Aerosol–ice formation closure: A southern great plains field campaign. *Bulletin of the American Meteorological Society*, *102*(10), E1952–E1971.

Korolev, A., McFarquhar, G., Field, P. R., Franklin, C., Lawson, P., Wang, Z., ... others (2017). Mixed-phase clouds: Progress and challenges. *Meteorological Monographs*, *58*, 5–1.

Krishnamoorthy, K., & Lee, M. (2013). New approximate confidence intervals for the difference between two poisson means and comparison. *Journal of Statistical Computation and Simulation*, *83*(12), 2232–2243.

McCluskey, C. S., DeMott, P. J., Ma, P.-L., & Burrows, S. M. (2019). Numerical representations of marine ice-nucleating particles in remote marine environments evaluated against observations. *Geophysical Research Letters*, *46*(13), 7838–7847.

McCluskey, C. S., Hill, T. C., Sultana, C. M., Laskina, O., Trueblood, J., Santander, M. V., ... others (2018). A mesocosm double feature: Insights into the chemical makeup of marine ice nucleating particles. *Journal of the Atmospheric Sciences*, *75*(7), 2405–2423.

Möhler, O., Adams, M., Lacher, L., Vogel, F., Nadolny, J., Ullrich, R., ... others (2021). The portable ice nucleation experiment (pine): a new online instrument for laboratory studies and automated long-term field observations of ice-nucleating particles. *Atmospheric Measurement Techniques*, *14*(2), 1143–1166.

Neale, R. B., Chen, C.-C., Gettelman, A., Lauritzen, P. H., Park, S., Williamson, D. L., ... others (2010). Description of the ncar community atmosphere model (cam 5.0). *NCAR Tech. Note NCAR/TN-486+ STR*, *1*(1), 1–12.

Pruppacher, H. R., Klett, J. D., & Wang, P. K. (1998). *Microphysics of clouds and precipitation.* Taylor & Francis.

Raman, A., Hill, T., DeMott, P., Singh, B., Zhang, K., Ma, P.-L., ... Burrows, S. (2022). Long-term variability in immersion-mode marine ice nucleating particles from climate model simulations and observations. *Atmospheric Chemistry and Physics Discussions*, 1–36.

Reicher, N., Budke, C., Eickhoff, L., Raveh-Rubin, S., Kaplan-Ashiri, I., Koop, T., & Rudich, Y. (2019). Size-dependent ice nucleation by airborne particles during dust events in the eastern mediterranean. *Atmospheric Chemistry and Physics*, *19*(17), 11143–11158.

Sullivan, R., Petters, M. D., DeMott, P. J., Kreidenweis, S. M., Wex, H., Niedermeier, D., ... others (2010). Irreversible loss of ice nucleation active sites in mineral dust particles caused by sulphuric acid condensation. *Atmospheric Chemistry and Physics*, *10*(23), 11471–11487.

Tan, I., Barahona, D., & Coopman, Q. (2022). Potential link between ice nucleation and climate model spread in arctic amplification. *Geophysical Research Letters*, *49*(4), e2021GL097373.

Testa, B., Hill, T. C., Marsden, N. A., Barry, K. R., Hume, C. C., Bian, Q., ... others (2021). Ice nucleating particle connections to regional argentinian land surface emissions and weather during the cloud, aerosol, and complex terrain interactions experiment. *Journal of Geophysical Research: Atmospheres*, *126*(23), e2021JD035186.

Tian, Y., Peters-Lidard, C. D., Eylander, J. B., Joyce, R. J., Huffman, G. J., Adler, R. F., ... Zeng, J. (2009). Component analysis of errors in satellite-based precipitation estimates. *Journal of Geophysical Research: Atmospheres*, *114*(D24).

Ullrich, R., Hoose, C., Möhler, O., Niemand, M., Wagner, R., Höhler, K., ... Leisner, T. (2017). A new ice nucleation active site parameterization for desert dust and soot. *Journal of the Atmospheric Sciences*, *74*(3), 699–717.

Vali, G., DeMott, P., Möhler, O., & Whale, T. (2015). A proposal for ice nucleation terminology. *Atmospheric Chemistry and Physics*, *15*(18), 10263–10270.

Vergara-Temprado, J., Miltenberger, A. K., Furtado, K., Grosvenor, D. P., Shipway, B. J., Hill, A. A., ... Carslaw, K. S. (2018). Strong control of southern ocean cloud reflectivity by ice-nucleating particles. *Proceedings of the National Academy of Sciences*, *115*(11), 2687–2692.

Wang, H., Easter, R., Zhang, R., Ma, P.-L., Singh, B., Zhang, K., ... others (2020). Aerosols in the e3sm version 1: New developments and their impacts on radiative forcing. *Journal of Advances in Modeling Earth Systems*, *12*(1), e2019MS001851.

Wang, Y., Zheng, X., Dong, X., Xi, B., Wu, P., Logan, T., & Yung, Y. L. (2020). Impacts of long-range transport of aerosols on marine-boundary-layer clouds in the eastern north atlantic. *Atmospheric Chemistry and Physics*, *20*(23), 14741–14755.

Wu, M., Liu, X., Yu, H., Wang, H., Shi, Y., Yang, K., ... others (2020). Understanding processes that control dust spatial distributions with global climate models and satellite observations. *Atmospheric Chemistry and Physics*, *20*(22), 13835–13855.

Zelinka, M. D., Zhou, C., & Klein, S. A. (2016). Insights from a refined decomposition of cloud feedbacks. *Geophysical Research Letters*, *43*(17), 9259–9269.

Zhang, K., Zhang, W., Wan, H., Rasch, P. J., Ghan, S. J., Easter, R. C., ... others (2022). Effective radiative forcing of anthropogenic aerosols in e3sm version 1: historical changes, causality, decomposition, and parameterization sensitivities. *Atmospheric Chemistry and Physics*, *22*(13), 9129–9160.

Zhang, S., Zhang, K., Wan, H., & Sun, J. (2022). Further improvement and evaluation of nudging in the e3sm atmosphere model version 1 (eamv1). *Geoscientific Model Development Discussions*, 1–37.

Zhang, Y., Ye, A., Nguyen, P., Analui, B., Sorooshian, S., & Hsu, K. (2021). New insights into error decomposition for precipitation products. *Geophysical Research Letters*, *48*(17), e2021GL094092.

Zheng, G., Wang, Y., Aiken, A. C., Gallo, F., Jensen, M. P., Kollias, P., ... others (2018). Marine boundary layer aerosol in the eastern north atlantic: seasonal variations and key controlling processes. *Atmospheric Chemistry and Physics*, *18*(23), 17615–17635.

Disentangling The Causes of Discrepancies In Simulated Immersion-mode Ice Nucleating Particles

Aishwarya Raman [1], Elise K. Wilbourn [2,3], Mikhail S. Pekour[1], Naruki Hiranuma [2], Susannah M. Burrows[1]

[1]Pacific Northwest National Lab, Richland, WA
[2]Dept. of Life, Earth and Environmental Sciences, West Texas A&M University,Canyon, TX
[3]*Now at Sandia National Laboratories,Livermore, CA

Key Points:

- Global climate model simulated immersion-mode INP concentrations are one to three orders of magnitude lower than INP measurements.
- Aerosol-INP closure is achieved (INPs within a factor of 10) for INPs simulated using the in situ aerosol measurements
- Errors in the model-simulated aerosol properties are the dominant cause of the model INP discrepancy .

Abstract

We assess the predictability of immersion-mode ice nucleating particles (INPs) at a remote marine site in the Eastern North Atlantic (ENA) using aerosol simulations from a global climate model as inputs to the immersion-mode INP parameterizations. While the model-simulated INP concentrations are lower by one to three orders of magnitudes compared to the measurements, we achieve aerosol-INP closure at ENA using the observed aerosol properties. We demonstrate a novel INP error decomposition approach to quantify the portion of total INP error from different error components. We conclude that inaccuracies in aerosols (surface area and composition) are the dominant cause of the model INP discrepancy at ENA. We recommend that, for future aerosol-INP closure studies, along with the measurements for total INP concentrations, campaigns should also collect co-located aerosol size-resolved composition measurements (in the INP-relevant size range) to better distinguish and quantify the error sources.

Plain Language Summary

We assess the predictability of ice nucleating particles (INPs) at a remote marine site in the Eastern North Atlantic (ENA) using aerosol simulations from a global climate model as inputs to the immersion-mode INP parameterizations. Model-simulated INP concentrations at ENA are lower by one to three orders of magnitude compared to the measurements. However, INPs predicted using the observed aerosol properties are within an order of magnitude from INP measurements. We quantify the portion of errors from aerosol and INP parameterization components. We conclude that inaccuracies in aerosol surface area and composition are the dominant causes for the model INP discrepancy at ENA.

1 Introduction

Mixed-phase clouds (MPCs) play a vital role in precipitation and radiation budget due to the presence of super-cooled liquid water and ice crystals (Korolev et al., 2017; Burrows et al., 2022). The dominant mechanism for heterogeneous ice formation in MPCs is the immersion-mode freezing of cloud droplets in the presence of ice nucleating particles (INPs) at temperatures warmer than $-38\,^{\circ}\mathrm{C}$ (Pruppacher et al., 1998; Vali et al., 2015). INPs are a rare subset of aerosols whose ice nucleating ability depends on the size-resolved particle composition, abundance, surface properties, and atmospheric conditions (e.g. DeMott et al., 2010; Boose et al., 2016).

In general, the INP number concentrations in the marine atmosphere are lower by an order of magnitude or more compared to those in terrestrial regions (e.g. DeMott et al., 2016). However, sea spray (salt + organics) emitted from bubble bursting in the ocean and mineral dust transported to the marine atmosphere from deserts can significantly affect the INP population in the marine boundary layer (e.g. Creamean et al., 2019; McCluskey et al., 2019). Previous studies over remote marine regions have shown that presence of INPs can alter climate feedbacks (e.g. Vergara-Temprado et al., 2018; Tan et al., 2022), but climate models can exhibit significant bias in prediction of INPs (Raman et al., 2022).

The predictive understanding of INPs in climate models is limited by sparse measurements of co-located aerosol size-resolved composition and INP number concentration. Recent INP studies have resorted to aerosol-INP closure experiments to investigate the error sources in INP prediction. Aerosol-INP closure for a given INP measurement temperature is defined as the agreement between the predicted INPs from observed aerosol properties and the measured INP concentrations within measurement uncertainties (Burrows et al., 2022). Knopf et al. (2021) conducted aerosol-INP closure during a frontal passage at the Department of Energy (DOE) site in the Southern Great Plains, and found that size-resolved INP com-

position and individual INP propensity are especially important for closure in regions with frequent variations in meteorological and aerosol conditions.

In this study, we assess the dominant cause of errors in the boundary-layer immersion-mode INP predictability during the DOE field campaign, Examining the Ice Nucleating Particles from the Eastern North Atlantic (ExINP-ENA), from October 2020 to December 2020 (Hiranuma et al., 2022). We perform aerosol-INP closure at ENA (39.09°N, 28.02°W) (Text S1) and constrain the spread in modeled INP concentrations using different aerosol measurements and INP parameterizations. We introduce a novel error decomposition approach to quantify the portion of total INP discrepancy between model and observations associated with individual error sources. We illustrate the methods for the aerosol-INP closure and INP error decomposition in Section 2, describe and discuss our findings in Section 3 and Section 4.

2 Methods

2.1 Aerosol and INP Measurements

We summarize the suite of aerosol and INP measurements in Table S1. We estimate the total aerosol surface area per unit volume (S_{aer} [$m^2\,m^{-3}$]) and related uncertainties using the ARM Aerosol Observing System (AOS) nephelometer-based aerosol scattering efficiency measurements (DeMott et al., 2016; Testa et al., 2021) at 450 nm wavelength (Text S3). We calculate six hourly averages of S_{aer} estimates to match time stamps in the INP measurements. For particle-type classification, we use the elemental composition data (based on 100 particle samples) from scanning electron microscopy coupled with energy-dispersive X-ray spectroscopy (SEM-EDX) (China et al., 2017). We estimate the total atomic weight proportion for dust and sea spray particles using the classification techniques in Cheng et al. (2016) and Hiranuma et al. (2013) (Text S4 and Table S2).

We use immersion mode ambient INP number concentrations measured with the Portable Ice Nucleation Experiment (PINE) chamber (Bilfinger Noel, model PINE-3) (Möhler et al., 2021) at temperatures between $-14\,°C$ and $-33\,°C$. INP concentrations were measured approximately every 12 minutes, and measurements were averaged for six hours to obtain adequate sampling statistics in a clean marine environment. We derive temperature-dependent errors for INP concentrations (Hiranuma et al., 2022) in terms of a 95% confidence interval (CI) using the Poisson statistics (Krishnamoorthy & Lee, 2013) (Text S6).

2.2 Model Overview and INP Parameterizations

We use the U.S. DOE Energy Exascale Earth System Atmosphere Model version 1 (EAMv1) (Neale et al., 2010; Golaz et al., 2022) with the modal aerosol module with four log-normal modes (MAM4) (H. Wang et al., 2020) to simulate the size-resolved aerosol composition inputs for the INP parameterizations. We provide more details about the EAMv1 model in Text S7.

We quantify the IN efficiency ($n_s(T)$ [INP concentrations per unit area, m^{-2}]) for dust and sea spray INPs using the temperature-dependent ice nucleation active site (INAS) parameterizations (Table S3). We derive INP concentrations by multiplying the $n_s(T)$ estimates with dust/sea spray surface area, depending on the INP type.

We include only dust and sea spray INPs at ENA because these two aerosol types have been commonly observed at ENA in previous studies (Y. Wang et al., 2020; Zheng et al., 2018). We estimate sea spray $n_s(T)$ following McCluskey et al. (2018). For dust INPs, we use multiple $n_s(T)$ parameterizations: Boose et al. (2016) (B16 Morocco, B16 Pelopennese),

Ullrich et al. (2017) (UL17), and Reicher et al. (2019) (REI19 super-micron) (Text S8 and Text S9).

2.3 Experiment Design and INP Closure

We ran EAMv1 simulations for the period of January-December 2020 with approximately 100 km horizontal resolution and 72 vertical layers using prescribed sea surface temperature and constrained meteorology (S. Zhang et al., 2022). We nudged the model winds at all model vertical levels using the Modern-Era Retrospective Analysis for Research and Applications, version 2 (MERRA-2) reanalysis data (Gelaro et al., 2017) at a 6-h relaxation time scale.

To permit spatial and temporal co-location between model outputs and INP measurements, we use the simulated aerosol fields at the nearest model grid box to the ENA station and use the 6-hourly averaged model outputs to estimate INP concentrations. We calculate the INP concentrations offline (i.e. model cloud microphysics is not affected by the INPs simulated in this study) by using the EAMv1-simulated and co-located dust and sea spray aerosols and the INP parameterizations.

We characterize the INP discrepancy between EAMv1-predicted INPs and PINE measurements in terms of modified normalized bias (MNB) (Equation 1), which is calculated as the difference in two quantities divided by the sum of the quantities (Text S10). Equation 1 shows a general formula for estimating MNB from two INP calculations, $\mathrm{INP}_1(T)$ and $\mathrm{INP}_2(T)$.

$$\mathrm{MNB}\left(\mathrm{INP}_1(T), \mathrm{INP}_2(T)\right) = \frac{\mathrm{INP}_1(T) - \mathrm{INP}_2(T)}{\mathrm{INP}_1(T) + \mathrm{INP}_2(T)}\,. \tag{1}$$

To quantify the aerosol-INP closure (schema in Figure S3), we estimate INP concentrations using the observed aerosol properties ('closure INPs'), nephelometer-estimated S_{aer} and the SEM-EDX derived fraction of dust and sea spray in the total chemical composition for 100 SEM-EDX samples. We declare aerosol-INP closure if the closure INP estimates are within a factor of 10 from the measurements. We express the closure error using the MNB metric.

Several climate modeling studies in the literature have adopted error decomposition techniques to determine the dominant processes contributing to bias in GCM simulated feedbacks (e.g. Tian et al., 2009; Y. Zhang et al., 2021; Zelinka et al., 2016). For a given INP measurement temperature, we express the total predicted INP discrepancy (E_p) as a linear combination of three error sources: the portion of E_p associated with S_{aer} ($E_{S_{aer}}$), composition (E_c), and residual sources (E_{res}) (Equation 2). Finally, we quantify the uncertainty in each error source given the independent aerosol and INP measurements, each with an uncertainty (Table 2). We use an uncertainty propagation technique to quantify the uncertainties in E_c and E_{res} (Text S11).

$$E_{\mathrm{p}} = E_{\mathrm{Saer}} + E_{\mathrm{c}} + E_{\mathrm{res}}\,. \tag{2}$$

3 Results

3.1 Comparing Simulated and Observed Aerosol Properties

Figure 1 compares the co-located surface level dust (Figure 1a), sea spray (Figure 1b), and total surface area (Figure 1c) from EAMv1 simulations and in situ measurements at ENA.

Experiment name	**Surface area**	**Aerosol composition**
INP E3SM	S_{aer} from E3SM for the size range $0.08 - 10\mu m$	E3SMv1 simulations of dust and sea spray aerosol fractions
INP E3SM NEPH	Dust and sea spray aerosol surface were calculated using S_{aer} from the AOS nephelometer	E3SMv1 simulations of dust and sea spray aerosol fractions
INP EDX E3SM	S_{aer} from E3SMv1	Aerosol fraction for dust and sea spray from SEM-EDX
INP EDX NEPH	S_{aer} from the nephelometer	Aerosol fraction for dust and sea spray from SEM-EDX

Table 1. INP calculations using various observed and simulated aerosol quantities.

Overall, the EAMv1-simulated surface area estimates are typically lower by one to two orders of magnitude compared to the in situ measurements. For the particle-type fraction, EAMv1 overestimates sea spray fraction and underestimates dust fraction compared to SEM-EDX measurements, both approximately by an order of magnitude. To better understand the aerosol classification at ENA, we compare our SEM-EDX classification with Knopf et al., 2022 analysis at the ENA site (Text S5).

The biases in EAMv1-simulated aerosols over the remote marine regions are mainly due to the high vertical resolution and higher dry deposition rates in the model (a factor of two compared to CAM5 and other AeroCom (Aerosol Comparisons Observations and Models) models) (Wu et al., 2020; Feng et al., 2022). Such biases in dry deposition velocities are not uncommon to global models (e.g. Emerson et al., 2020). In addition to dry deposition, aerosol biases in EAMv1 are also affected by biases in other physical processes such as aerosol wet scavenging (K. Zhang et al., 2022). In marine regions where INP concentrations are already lower compared to continental regions, systematic differences between the simulated and observed aerosol surface area and composition as large as two orders of magnitude will directly affect the magnitude of INPs estimated using the simulated aerosol quantities.

3.2 INP Concentrations at ENA

Figure 2 compares the 6-hourly averaged INP number concentration measurements from PINE with EAMv1-simulated (and co-located) dust and sea spray INP concentrations for different measurement temperatures. The lack of strong seasonal variability in the INP measurements at ENA suggests that dust and sea spray INPs are persistent INP sources throughout the year. The INP number concentration measurements over the study period range from $0.1\,\mathrm{L}^{-1}$ to $100\,\mathrm{L}^{-1}$ for temperatures between $-20\,^{\circ}\mathrm{C}$ and $-30\,^{\circ}\mathrm{C}$ respectively. However, INP E3SM estimates (Blue lines in Figure 2) are generally lower by one to two orders of magnitudes compared to the INP measurements. We find that combining EAMv1-simulated sea spray (M18) and dust INPs provides little improvement in the model-observation discrepancy at ENA.

Among the dust INP parameterizations (Table S3), UL17, B16 Pelopennese, and B16 Morocco show the maximum, median, and minimum discrepancies with measurements, respectively. Higher INP concentrations in B16 Morocco are likely due to the higher IN propensity of milled dust samples used for the development of the parameterization (Boose et al., 2016). Milling increases the surface irregularities, which in turn increases the IN activity (Reicher et al., 2019). Given these caveats about the IN efficiency of milled dust samples, it is possible that the good agreement between simulated B16 Morocco INPs and PINE measurements at ENA is likely due to the compensating errors between dust surface area underestimation in EAMv1 and $n_s(T)$ overestimation in B16 Morocco.

Error source / Calculation	**Purpose**	**Uncertainty calculation**
$E_p = \mathrm{MNB}(\mathrm{INP}_{\mathrm{E3SM}}, \mathrm{INP}_{\mathrm{OBS}})$	Total predictive skill error for E3SM v1 simulated vs. observed INP concentrations	Associated with different dust INP parameterizations.
$E_{S_{\mathrm{aer}}} = \mathrm{MNB}(\mathrm{INP}_{\mathrm{E3SM}}, \mathrm{INP}_{\mathrm{E3SM\ NEPH}})$	Portion of E_p associated with mismatch in simulated and observed S_{aer}	Calculated using uncertainties in the nephelometer scattering coefficients, Q (lower bound = 0.42, upper bound = 3.0).
$E_{\mathrm{c}} = \mathrm{MNB}(\mathrm{INP}_{\mathrm{E3SM\ NEPH}}, \mathrm{INP}_{\mathrm{EDX\ NEPH}})$	Portion of $E_{S_{aer}}$ associated with mismatch in E3SMv1 simulated vs. observed aerosol composition.	Calculated by propagating standard errors in SEM-EDX aerosol fraction to MNMB. For E3SM NEPH, we use a median Q = 2.0.
$E_{\mathrm{res}} = \mathrm{MNB}(\mathrm{INP}_{\mathrm{EDX\ NEPH}}, \mathrm{INP}_{\mathrm{OBS}})$	Residual errors (e.g., missing INP sources, errors in INP parameterizations, and atmospheric transformation of INPs.)	Calculated by propagating temperature dependent errors in measurements to MNMB. We use a median dust and sea spray fraction from EDX.

Table 2. INP error decomposition and uncertainty calculation for individual error components

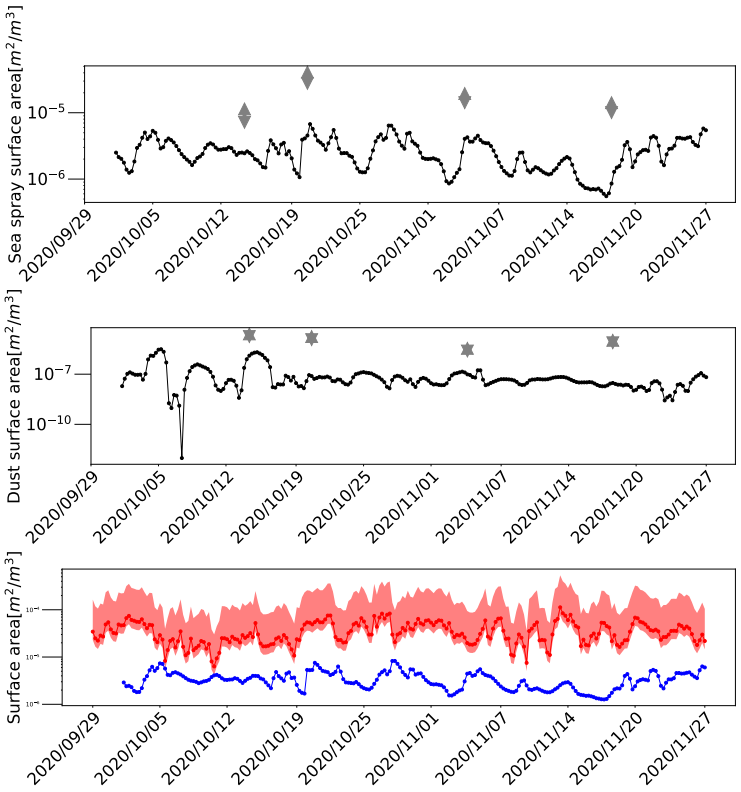

Figure 1. (a) Simulated (black) and observed (grey) dust surface area from E3SMv1 simulations and SEM-EDX (dust fraction) + Nephelometer (total surface area), respectively, along with the measurement uncertainties. (b) Same as (a) but comparing observations and model for sea spray aerosol surface area. (c) Simulated (blue) and observed (red) total surface area from E3SMv1 and the Nephelometer, respectively, along with the Nephelometer surface area uncertainties (red shaded region) calculated using the upper (3.0) and lower (0.42) bound for assumptions of scattering coefficients. Surface area estimates shown here for EAMv1 cover the size range 80 nm to 10 µm. In panels (a) and (b), observed surface area for dust and sea spray was estimated using the SEM-EDX particle-type classification. Each SEM-EDX measurement represents a sampling period of two to three days. To calculate the dust and sea spray surface area using the SEM-EDX particle-type classification data, we used the total surface area from the Nephelometer corresponding to the last day of the SEM-EDX measurement.

Overall, the uncertainty in the model discrepancies for different INP parameterizations is in the same order of magnitude as the discrepancy due to the simulated aerosol properties (Figure 2, blue and red lines). This leads to the next question, what is the dominant cause of the model INP discrepancies at ENA - aerosol errors or deficiencies in the INP parameterizations?

3.3 INP Closure, Error Decomposition, and Uncertainty Propagation

Figure 2 compares the closure INPs (green squares) predicted using the observed aerosol properties against the EAMv1-simulated (blue) and measured (black) INP concentrations. We find that adding sea spray and dust INPs does not reduce the closure. The closure INPs (Figure 2, green squares) are within an order of magnitude from the PINE measurements, the criterion we use in this study for aerosol-INP closure. These results confirm that the

[ht]

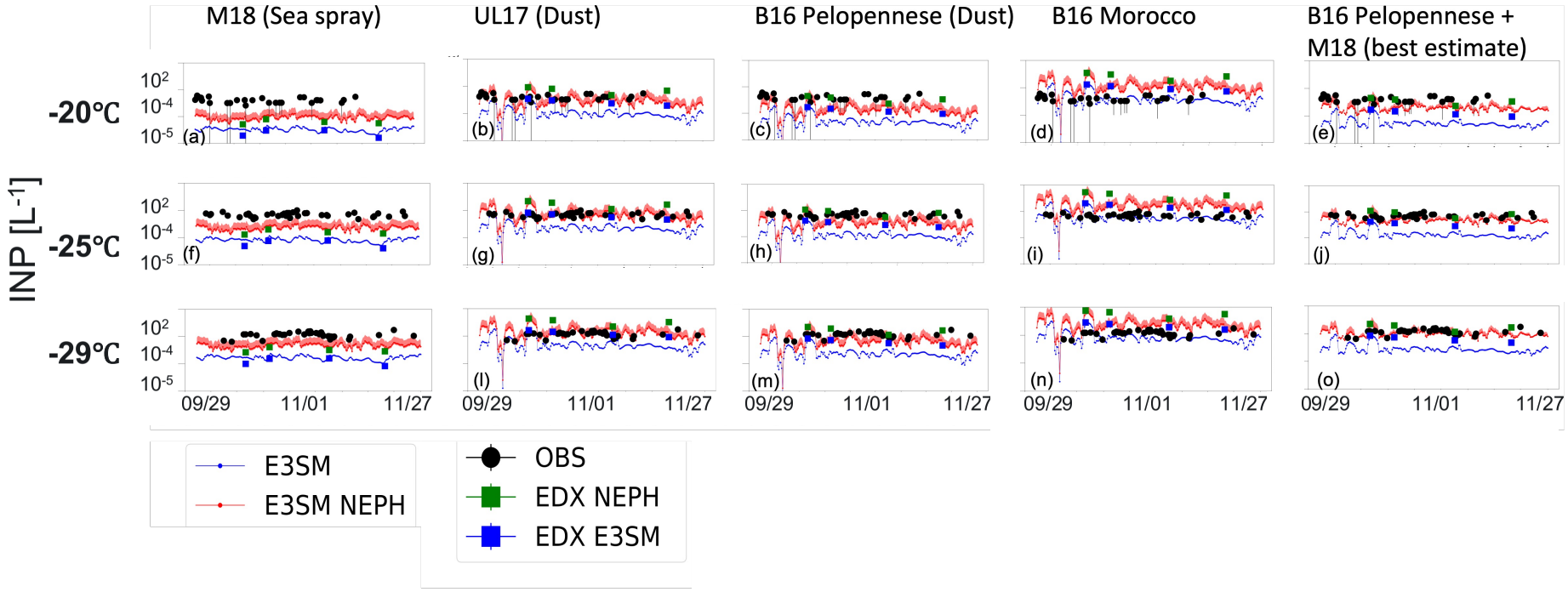

Figure 2. Time series of observed and modeled INP concentrations at −20°C,−25°C and −29°C. INP concentrations from PINE observations (ENA OBS) are shown as black circles. Different INP calculations are listed in Table 1.

EAMv1-simulated INP discrepancies as high as two to three orders of magnitude cannot be explained only by the deficiencies in the INP parameterizations.

Figure 3 illustrates the decomposition of model INP discrepancies (E_p) into error components associated with the simulated surface area ($E_{S_{aer}}$), composition (E_c), and the residual sources (closure error) (E_{res}). We find that $E_{S_{aer}}$+ E_c together estimate 20-30% higher median MNB compared to the MNB for E_{res}. The opposite signs for E_{res} and aerosol components ($E_{S_{aer}}$ and E_c) indicate that these two error sources partially compensate for one another. Therefore, improving only the INP parameterization errors without improving the aerosol errors in the model simulations will result in compensating biases in the model-predicted INPs.

We conclude that the inaccuracies in aerosol surface area and composition simulated in EAMv1 are the major reasons for the large discrepancy in model-predicted INP concentrations during the ExINP-ENA campaign. Along with improving the representation of aerosol properties in the model, accounting for deficiencies in the INP parameterizations by including missing INP sources and INP chemistry (e.g. biological INPs, coating of dust by sulfuric acid (Huang et al., 2021; Sullivan et al., 2010)) can further improve the INP closure at ENA.

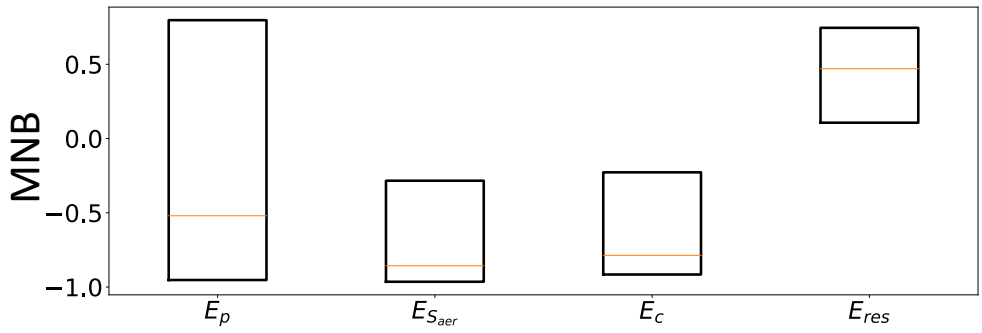

Figure 3. Decomposition of total INP discrepancies (dust and sea spray) at −29°C into individual error components, $E_{S_{aer}}$, E_c, and E_{res}. Table 2 describes the error components and uncertainties. The uncertainties in E_p are from using different dust INP parameterizations. For other error components, we show results only for the B16 Peloponnese + M18 INPs which have the least closure error compared to other dust parameterizations. Different nephelometer surface area estimates are derived based on the uncertainties in the scattering coefficient assumptions. The MNB range in $E_{S_{aer}}$ corresponds to using the lower and upper bound for nephelometer-derived surface area estimates in the INP parameterizations. Due to the limited number of temporally coincident observations from EDX, Neph, and PINE, sampling days for error sources are not the same. The number of days used for the calculation of E_p and $E_{S_{aer}}$ and their associated uncertainties are: 238 and 226. E_c and E_{res} represent four coincident SEM-EDX and INP samples. Upper and lower bounds for E_c are calculated using the variability in EDX errors in dust and sea spray fractions for different days during the campaign. We calculate E_{res} only for −29°C because of the limited availability of coincident measurements for SEM-EDX particle-type classification, PINE INP measurements, and temperature-dependent INP measurement errors at this temperature.

4 Discussion and Conclusion

In this study, we have investigated the predictive capability of EAMv1 and INAS-based INP parameterizations to simulate immersion-mode INP concentrations during the ExINPENA campaign at ENA, with an eye towards determining the leading cause of model-observation INP discrepancies. The EAMv1-simulated INP concentrations are one to three orders of magnitude lower than the INP measurements from PINE. We achieve INP closure (INP discrepancy within a factor of 10) when INPs are predicted using the measured aerosol properties from the AOS nephelometer and SEM-EDX. This evidence confirms that we cannot reduce such large discrepancies in the predicted INPs only by resolving the flaws in the INP parameterizations, but it is important to accurately represent the aerosol properties in the model to improve INP predictions.

We have demonstrated a novel INP error decomposition to quantify the portion of total INP model-observation discrepancies from different error sources. At the ENA site, we find that the inaccuracy in the EAMv1-simulated aerosol properties is the leading cause for the model INP discrepancies. Therefore, we conclude that correctly simulating the aerosol physical and chemical processes in the model is critical for accurately predicting the immersion-mode INP concentrations at ENA.

We note below some caveats of this study and their implications for the results. We used EAMv1-simulated aerosols for particle size range from 80 nm to 10 µm, whereas, PINE INP measurements are sensitive only up to 3 µm. Additionally, SEM-EDX size distribution data for ENA (for 100 samples) showed that only 10 to 17% of the surface area is between 3 µm and 5 µm. Therefore, almost an order of magnitude difference between the observed and simulated INPs cannot be attributed predominantly to the differences in the size cut off between PINE and the nephelometer.

We demonstrated the INP error decomposition method only for $-29\,^{\circ}\mathrm{C}$, because we did not have co-located SEM-EDX and INP measurements for other temperatures. Although we have considered only the temperature-dependent errors associated with counting statistics in the closure calculations, we recognize that other systematic uncertainties (e.g. loss of larger ice crystals between the PINE chamber and the optical counter, overlap in the size distribution of smaller ice crystals with the larger particles not activated to droplets) can also affect the INP measurements. Möhler et al. (2021) showed that for immersion freezing of mineral dust aerosols, PINE INP measurements were within the experimental uncertainties (%20) of the INP measurements from the Aerosol Interaction and Dynamics in the Atmosphere cloud chamber experiments.

Despite these caveats, this study provides key insights into the dominant sources of errors in immersion-mode INPs in the EAMv1 climate model. The INP error decomposition method we have demonstrated here can be modified and applied to other regions and field experiments. The information gained from the decomposition enables us to make recommendations for both model development and future field campaigns.

Improving INPs in climate models can significantly impact the simulated super-cooled liquid water (SLW) in MPC clouds, albedo, and climate. For example, a global climate modeling study found that with fewer INPs, the negative cloud-phase feedback was weakened, and strongly impacting the sea ice loss and Arctic Amplication (Tan et al., 2022). Overall, by better diagnosing and reducing the causes of INP errors, we can improve confidence in the use of aerosol-aware INP parameterizations in climate models and consequently reduce uncertainites in climate predictions (Burrows et al., 2022).

Acknowledgments

A. Raman thanks Catherine L. Himes from the PNNL communication team for technical editing support. A. Raman and S.M. Burrows were funded by the U.S. Department of Energy (DOE), Office of Science, Office of Biological and Environmental Research through the Early Career Research Program. N.Hiranuma and E.K.Wilbourn were funded under the DOE grant DE-SC-0018979. The Pacific Northwest National Laboratory is operated for DOE by Battelle Memorial Institute under contract DE-1713 AC05-76RL01830. E. K. Wilbourn and High-performance computing resources for this project was provided by the PNNL Research Computing, and the National Energy Research Scientific Computing Center (NERSC), a DOE Office of Science User Facility supported by the Office of Science of the U.S. Department of Energy under Contract No. DE-AC02-05CH11231.

Data Availability Statement E3SMv1 model simulated and co-located aerosol and INP data at ENA, SEM-EDX observations, nephelometer-based surface area estimates, and the corresponding Python scripts used for the analysis are available in the Zenodo repository DOI:10.5281/zenodo.7746607. PINE INP observations are archived in the ARM repository `https://www.arm.gov/research/campaigns/ena2020exinpena`. Aerosol scattering measurements from the Nephelometer are available in the ARM archive `https://adc.arm.gov/discovery/#/results/s::nephelometer`

Supporting Information ENAGRLSIworking.pdf

References

Boose, Y., Welti, A., Atkinson, J., Ramelli, F., Danielczok, A., Bingemer, H. G., ... Lohmann, U. (2016). Heterogeneous ice nucleation on dust particles sourced from nine deserts worldwide–part 1: Immersion freezing. *Atmospheric Chemistry and Physics*, *16*(23), 15075–15095.

Burrows, S. M., McCluskey, C. S., Cornwell, G., Steinke, I., Zhang, Kai, ... others (2022). Ice-nucleating particles that impact clouds and climate: Observational and modeling research needs. *Reviews of Geophysics*, e2021RG000745.

Cheng, C.-L., Chang, H.-H., Chen, T.-H., Tsai, P.-J., Huang, Y.-T., Huang, P.-J., & Lin, S.-Y. (2016). Spectral and morphological classification of different chronic and acute taiwanese gallstones via ftir, sem and esem-edx microanalyses. *Digestive and Liver Disease*, *48*(5), 519–527.

China, S., Alpert, P. A., Zhang, B., Schum, S., Dzepina, K., Wright, K., ... others (2017). Ice cloud formation potential by free tropospheric particles from long-range transport over the northern atlantic ocean. *Journal of Geophysical Research: Atmospheres*, *122*(5), 3065–3079.

Creamean, J., Cross, J. N., Pickart, R., McRaven, L., Lin, P., Pacini, A., ... others (2019). Ice nucleating particles carried from below a phytoplankton bloom to the arctic atmosphere. *Geophysical Research Letters*, *46*(14), 8572–8581.

DeMott, P. J., Hill, T. C., McCluskey, C. S., Prather, K. A., Collins, D. B., Sullivan, R. C., ... others (2016). Sea spray aerosol as a unique source of ice nucleating particles. *Proceedings of the National Academy of Sciences*, *113*(21), 5797–5803.

DeMott, P. J., Prenni, A. J., Liu, X., Kreidenweis, S. M., Petters, M. D., Twohy, C. H., ... Rogers, D. (2010). Predicting global atmospheric ice nuclei distributions and their impacts on climate. *Proceedings of the National Academy of Sciences*, *107*(25), 11217–11222.

Emerson, E. W., Hodshire, A. L., DeBolt, H. M., Bilsback, K. R., Pierce, J. R., McMeeking, G. R., & Farmer, D. K. (2020). Revisiting particle dry deposition and its role in radiative effect estimates. *Proceedings of the National Academy of Sciences*, *117*(42), 26076–26082.

Feng, Y., Wang, H., Rasch, P., Zhang, K., Lin, W., Tang, Q., ... Yu, H. (2022). Global dust cycle and direct radiative effect in e3sm version 1: Impact of increasing model resolution. *Journal of Advances in Modeling Earth Systems*, *14*(7), e2021MS002909.

Gelaro, R., McCarty, W., Suárez, M. J., Todling, R., Molod, A., Takacs, L., ... others (2017). The modern-era retrospective analysis for research and applications, version 2 (merra-2). *Journal of climate*, *30*(14), 5419–5454.

Golaz, J.-C., Van Roekel, L. P., Zheng, X., Roberts, A. F., Wolfe, J. D., Lin, W., ... others (2022). The doe e3sm model version 2: overview of the physical model and initial model evaluation. *Journal of Advances in Modeling Earth Systems*, *14*(12).

Hiranuma, N., Brooks, S. D., Moffet, R. C., Glen, A., Laskin, A., Gilles, M. K., ... McFarquhar, G. (2013). Chemical characterization of individual particles and residuals of cloud droplets and ice crystals collected on board research aircraft in the isdac 2008 study. *Journal of Geophysical Research: Atmospheres*, *118*(12), 6564–6579.

Hiranuma, N., Wilbourn, E. K., & Lacher, L. (2022). *Examining the ice-nucleating particles from the eastern north atlantic (exinp-ena) field campaign report* (Tech. Rep.). Oak Ridge National Lab.(ORNL), Oak Ridge, TN (United States). Atmospheric ....

Huang, S., Hu, W., Chen, J., Wu, Z., Zhang, D., & Fu, P. (2021). Overview of biological ice nucleating particles in the atmosphere. *Environment International*, *146*, 106197.

Knopf, D. A., Barry, K., Brubaker, T., Jahl, L., Jankowski, K., Li, J., ... others (2021). Aerosol–ice formation closure: A southern great plains field campaign. *Bulletin of the American Meteorological Society*, *102*(10), E1952–E1971.

Korolev, A., McFarquhar, G., Field, P. R., Franklin, C., Lawson, P., Wang, Z., ... others (2017). Mixed-phase clouds: Progress and challenges. *Meteorological Monographs*, *58*, 5–1.

Krishnamoorthy, K., & Lee, M. (2013). New approximate confidence intervals for the difference between two poisson means and comparison. *Journal of Statistical Computation and Simulation*, *83*(12), 2232–2243.

McCluskey, C. S., DeMott, P. J., Ma, P.-L., & Burrows, S. M. (2019). Numerical representations of marine ice-nucleating particles in remote marine environments evaluated against observations. *Geophysical Research Letters*, *46*(13), 7838–7847.

McCluskey, C. S., Hill, T. C., Sultana, C. M., Laskina, O., Trueblood, J., Santander, M. V., ... others (2018). A mesocosm double feature: Insights into the chemical makeup of marine ice nucleating particles. *Journal of the Atmospheric Sciences*, *75*(7), 2405–2423.

Möhler, O., Adams, M., Lacher, L., Vogel, F., Nadolny, J., Ullrich, R., ... others (2021). The portable ice nucleation experiment (pine): a new online instrument for laboratory studies and automated long-term field observations of ice-nucleating particles. *Atmospheric Measurement Techniques*, *14*(2), 1143–1166.

Neale, R. B., Chen, C.-C., Gettelman, A., Lauritzen, P. H., Park, S., Williamson, D. L., ... others (2010). Description of the ncar community atmosphere model (cam 5.0). *NCAR Tech. Note NCAR/TN-486+ STR*, *1*(1), 1–12.

Pruppacher, H. R., Klett, J. D., & Wang, P. K. (1998). *Microphysics of clouds and precipitation.* Taylor & Francis.

Raman, A., Hill, T., DeMott, P., Singh, B., Zhang, K., Ma, P.-L., ... Burrows, S. (2022). Long-term variability in immersion-mode marine ice nucleating particles from climate model simulations and observations. *Atmospheric Chemistry and Physics Discussions*, 1–36.

Reicher, N., Budke, C., Eickhoff, L., Raveh-Rubin, S., Kaplan-Ashiri, I., Koop, T., & Rudich, Y. (2019). Size-dependent ice nucleation by airborne particles during dust events in the eastern mediterranean. *Atmospheric Chemistry and Physics*, *19*(17), 11143–11158.

Sullivan, R., Petters, M. D., DeMott, P. J., Kreidenweis, S. M., Wex, H., Niedermeier, D., ... others (2010). Irreversible loss of ice nucleation active sites in mineral dust particles caused by sulphuric acid condensation. *Atmospheric Chemistry and Physics*, *10*(23), 11471–11487.

Tan, I., Barahona, D., & Coopman, Q. (2022). Potential link between ice nucleation and climate model spread in arctic amplification. *Geophysical Research Letters*, *49*(4), e2021GL097373.

Testa, B., Hill, T. C., Marsden, N. A., Barry, K. R., Hume, C. C., Bian, Q., ... others (2021). Ice nucleating particle connections to regional argentinian land surface emissions and weather during the cloud, aerosol, and complex terrain interactions experiment. *Journal of Geophysical Research: Atmospheres*, *126*(23), e2021JD035186.

Tian, Y., Peters-Lidard, C. D., Eylander, J. B., Joyce, R. J., Huffman, G. J., Adler, R. F., ... Zeng, J. (2009). Component analysis of errors in satellite-based precipitation estimates. *Journal of Geophysical Research: Atmospheres*, *114*(D24).

Ullrich, R., Hoose, C., Möhler, O., Niemand, M., Wagner, R., Höhler, K., ... Leisner, T. (2017). A new ice nucleation active site parameterization for desert dust and soot. *Journal of the Atmospheric Sciences*, *74*(3), 699–717.

Vali, G., DeMott, P., Möhler, O., & Whale, T. (2015). A proposal for ice nucleation terminology. *Atmospheric Chemistry and Physics*, *15*(18), 10263–10270.

Vergara-Temprado, J., Miltenberger, A. K., Furtado, K., Grosvenor, D. P., Shipway, B. J., Hill, A. A., ... Carslaw, K. S. (2018). Strong control of southern ocean cloud reflectivity by ice-nucleating particles. *Proceedings of the National Academy of Sciences*, *115*(11), 2687–2692.

Wang, H., Easter, R., Zhang, R., Ma, P.-L., Singh, B., Zhang, K., ... others (2020). Aerosols in the e3sm version 1: New developments and their impacts on radiative forcing. *Journal of Advances in Modeling Earth Systems*, *12*(1), e2019MS001851.

Wang, Y., Zheng, X., Dong, X., Xi, B., Wu, P., Logan, T., & Yung, Y. L. (2020). Impacts of long-range transport of aerosols on marine-boundary-layer clouds in the eastern north atlantic. *Atmospheric Chemistry and Physics*, *20*(23), 14741–14755.

Wu, M., Liu, X., Yu, H., Wang, H., Shi, Y., Yang, K., ... others (2020). Understanding processes that control dust spatial distributions with global climate models and satellite observations. *Atmospheric Chemistry and Physics*, *20*(22), 13835–13855.

Zelinka, M. D., Zhou, C., & Klein, S. A. (2016). Insights from a refined decomposition of cloud feedbacks. *Geophysical Research Letters*, *43*(17), 9259–9269.

Zhang, K., Zhang, W., Wan, H., Rasch, P. J., Ghan, S. J., Easter, R. C., ... others (2022). Effective radiative forcing of anthropogenic aerosols in e3sm version 1: historical changes, causality, decomposition, and parameterization sensitivities. *Atmospheric Chemistry and Physics*, *22*(13), 9129–9160.

Zhang, S., Zhang, K., Wan, H., & Sun, J. (2022). Further improvement and evaluation of nudging in the e3sm atmosphere model version 1 (eamv1). *Geoscientific Model Development Discussions*, 1–37.

Zhang, Y., Ye, A., Nguyen, P., Analui, B., Sorooshian, S., & Hsu, K. (2021). New insights into error decomposition for precipitation products. *Geophysical Research Letters*, *48*(17), e2021GL094092.

Zheng, G., Wang, Y., Aiken, A. C., Gallo, F., Jensen, M. P., Kollias, P., ... others (2018). Marine boundary layer aerosol in the eastern north atlantic: seasonal variations and key controlling processes. *Atmospheric Chemistry and Physics*, *18*(23), 17615–17635.

Supporting Information for "Disentangling The Causes of Discrepancies In Simulated Immersion-mode Ice Nucleating Particles"

Aishwarya Raman [1], Elise K. Wilbourn [2,3], Naruki Hiranuma [2], Mikhail S. Pekour[1], Susannah M. Burrows[1]

[1]Pacific Northwest National Lab, Richland, WA

[2]Dept. of Life, Earth and Environmental Sciences, West Texas A&M University,Canyon, TX

[3]*Now at Sandia National Laboratories,Livermore, CA

Contents of this file

1. Text S1 to S11
2. Figures S1 to S3
3. Dataset S1
4. Tables S1 to S4

Text S1. Sampling location

INP and aerosol measurements were sampled at the Department of Energy (DOE) Atmospheric Radiation Measurement (ARM) observatory in Graciosa Island, Azores (39.09°N, 28.02°W) (Hiranuma et al., 2022; Uin et al., 2020). The observatory is located in a remote marine setting in the Eastern North Atlantic (ENA), ca. 1500 km away from the nearest continental land mass and the island is surrounded by ocean waters rich in seasonal phytoplankton (Zawadowicz et al., 2021). The marine boundary layer at ENA is impacted by the oceanic emissions of sea spray aerosol and long-range-transported dust and continental aerosol (Logan et al., 2014).

Text S2. List of aerosol and INP measurements

Table S1 provides a summary of aerosol and INP instruments along with the particle size range detected by the instrument.

Text S3. Deriving total aerosol surface area From nephelometer

The integrating nephelometer is an instrument in the ARM Aerosol Observing System (AOS) at the ENA observatory that measures aerosol optical scattering in three wavelengths

Table S1. Measurable particle size range for individual instruments used in this study.

Instrument	Manufacturer-Model	Measurable size range (nm)
Nephelometer	TSI-3563	10-10000 (Volume Equivalent Diameter)
SEM-EDX	JEOL-JSM-6010LA	250-8000 (Area-equivalent Diameter – Aerodynamic Diameter)
PINE	Bilfinger Noell - PINE-3	30-3000 (Aerodynamic Diameter)

(700 nm, 500 nm, and 450 nm) at ambient relative humidity conditions. In this study, we use the total aerosol surface area per unit volume (S_{aer} in units of $m^2\,m^{-3}$) derived using the aerosol scattering coefficients at the wavelength λ= 450 nm.

$$S_{aer} = 4\frac{b_{sp}}{Q}\,, \tag{1}$$

where b_{sp} is the aerosol scattering coefficient (m^{-1}) measured by the nephelometer, and Q is the total aerosol scattering efficiency assumed based on the characteristic total aerosol distribution and composition. The AOS nephelometer alternates between a 1 µm impactor and a 10 µm impactor for measuring scattering from submicron and super-micron aerosol size distributions. Because ice nucleating efficiency of aerosol particles is directly proportional to their total surface area, we use scattering measurements only for larger particles from the 10 µm impactor with an aerodynamic diameter size cut off at 10 µm.

Approximations for Q values are based on the aerosol size distribution dominating scattering at a given location and time. Following DeMott et al. (2016), we assumed $Q = 3.0$ for marine aerosols with dominant scattering from submicron particles. Testa et al. (2021) estimated a range of Q values from 0.58–2.31 for sub- and supermicron particle size distributions at $\lambda = 450$ nm. To account for uncertainties in S_{aer} due to uncertainties in Q, we calculated S_{aer} for $Q = 0.58$, $Q = 2.0$, and $Q = 3.0$ using Equation 1.

Text S4. Particle-Type Classification using Scanning Electron Microscopy with Energy-Dispersive X-ray Analysis

Particle composition of aerosol particles collected from the Eastern North Atlantic (ENA) site was measured using the scanning electron microscopy energy dispersive X-ray spectroscopy (SEM-EDX) system (Jeol, last accessed, August 11 2022). SEM-EDX technology

is further described in the described in the manufacturer's online document (JEOL, 2022). Briefly, aerosol particles captured on polycarbonate filters were assessed with the SEM-EDX instrument to determine the atomic percentage (atomic %) of 13 elements (N, O, Na, Mg, Al, Si, P, S, Cl, K, Ca, Mn, and Fe). All analyses were consistently carried out with the electron beam accelerating voltage of 20 keV and a 10 mm distance from the underside of the SEM objective lens to the specimen surface. Since the particles were collected on polycarbonate filters, it was not possible to determine organic chemical composition. Instead, SEM-EDX data were used to determine the presence or absence of dust and/or sea salt particles. In addition, the relative age of the particle population was assessed by the ratio of Na+ to Cl-. For instance, this ratio in freshly emitted sea salt is typically much closer to that in the "aged" sea spray aerosols, which show depletion of chloride ions via reactions with sulfuric and nitric acid to form HCl aerosols (Zhang et al., 2010). Although this SEM-EDX method is qualitative rather than a quantitative measurement, atomic % and Na:Cl ratios can be used to determine the approximate amount of local, freshly emitted sea spray aerosols present at the ENA site as compared with the percentage of particles that are aged mixtures with dust.

A total of 400 aerosol particles (i.e., 4 filter samples and 100 particles per sample) in the observed diameter range up to 4.6 µm was analyzed on a single-particle basis (particle size distribution data is available upon request). It should be noted that, while the lower limit of particle collection is nominally 0.2 µm based on filter pore size, the lower detection limit for the SEM method employed here is 0.5 µm particle diameter. Single particles were selected on each filter to analyze particle composition, with at least 100 particles to represent the population chemical composition and allow for classification of major particle groups. All particles were randomly selected with a strategy of selecting 25 particles over the 128 µm x 96 µm cross-sections (x4). No specific particle size or shape was selected for analysis. Instead, a range of sizes and shapes was targeted to give the best approximation of overall population chemistry. SEM-EDX is a time-intensive and labor-intensive process, so its application during this study was limited. For this reason, a few time periods were chosen to study in greater detail. These periods contrast with one another in terms of ice-nucleating particle (INP) concentration and heat sensitivity (not shown). Each filter was collected for approximately four days and high INP periods were chosen based on complementary offline immersion freezing measurements. The same filters were analyzed with the offline cold stage-supported freezing assay measurements and SEM-EDX.

Data for each filter sample is available in Dataset S1. This table also shows the composition of samples determined with SEM-EDX. The atomic % of 13 different elements was used to classify particles as either salt-dominant (and thus marine-dominant) or dust-dominant (and thus terrestrial-dominant), classified based on methods presented in Figure 5 of Hiranuma et al. (2013).

The four sample periods were chosen to represent both high-INP periods ($0.39\,\mathrm{L}^{-1}$ and $0.33\,\mathrm{L}^{-1}$ at $-25\,^{\circ}\mathrm{C}$ for ENA2020-11 and ENA2020-14, respectively) and low INP periods ($0.04\,\mathrm{L}^{-1}$ and INP $0.1\,\mathrm{L}^{-1}$ at $-25\,^{\circ}\mathrm{C}$ for ENA2020-28 and ENA2020-36, respectively). Additionally, samples ENA2020-14 and ENA2020-36 showed heat sensitivity at temperatures above $-15\,^{\circ}\mathrm{C}$, while samples ENA2020-11 and ENA2020-28 did not heat sensitivity.

Most of the samples were dominated by salt-dominant particles, while ENA2020-11 had a greater percentage of dust-dominant particles. It is well-known that aluminosilicate mineral dust is capable of acting as an INP (Zimmermann et al., 2008) and generally does not show sensitivity to the heating method employed herein (Zolles et al., 2015). Although it is difficult to draw conclusions from a single sample, the high INP concentrations seen during this time period (and confirmed with online methods) could be due to higher concentrations of mineral dust in this sample than the others analyzed.

As seen in Dataset S1, the Na:Cl ratio in samples from ENA is consistently around 2. This number suggests that the samples are traveling from some distance and aging before reaching the site. However, since the site is 1500 km from the nearest sources of terrestrial material, sea spray aerosols must make up some proportion of the aerosols present at the site. The mixture of sea spray aerosols, dust, and organic material leads to a unique relationship between cloud condensation nuclei (CCN) and INPs at ENA that is heretofore unobserved at any other marine or terrestrial sites and suggests a common source for both types of aerosols. This relationship warranty further study and will be discussed in future papers.

Text S5. Comparison of SEM-EDX analysis to a previous aerosol classification study at ENA

Figure S1 shows the comparison of previous SEM-EDX-based particle composition data to our data for particle samples collected at the same location in ENA. Briefly, Knopf et al. (2022) (K22 hereafter) conducted the SEM-EDX-derived cluster analysis for the identifi-

cation of particle-type classes present in particle samples collected during the Aerosol and cloud experiments in ENA (ACE-ENA) campaign in June and July 2017. Panels (a–d) display the normalized atomic % of 13 selected elements for the four particle-type classes from ACE-ENA (adapted from K22). The representative particle types include (a) processed sea salt with mineral dust, sulfur, and organic matter, (b) sea salt particles, (c) processed sea salt with mineral dust, and (d) organic matter–chlorine-containing particles. Contrarily, Panels (e-h) show non-clustered atomic % of the same elements for individual samples from the Examining INP from ENA (ExINP-ENA) campaign in 2020 (i.e., Dataset S1). With notably high normalized atomic % of oxygen atoms (¿ 55 %), all ExINP-ENA samples indicate the inclusion of highly oxygenated sea salt- and dust-including particles. This oxygen-enriched feature can also be seen in Fig. S1a (processed sea salt with 50% oxygen atomic %). Likewise, the inclusion of sea salt- and dust-makers (i.e., Na, Mg, Cl, Al, and Ca) are commonly found in both ACE-ENA and ExINP-ENA samples. Although all aerosol particle populations analyzed from ExINP-ENA contained sea salt, all particles also contained dust in variable concentrations, and there was no relationship between air mass origin (determined by back-trajectory analysis but not shown) and dust content, indicating that all aerosol populations at ENA during the sampling period contained mixed sea spray aerosols and continental aerosols. While organic content could not be measured by SEM-EDX due to the background signal from the polycarbonate filter substrate, it is highly likely that the sea spray aerosols (indicated by the presence of Na and Cl in SEM-EDX) contained organic material in addition to salts since sea spray aerosols contain both salts and organic material. Such a high degree of mixed components can in part explain the observed indication of chloride depletion (Na:Cl ratios ¿ 1.9 in Table S1) and particle aging. On the other hand, our results generally suggest less inclusion of K, Mn, and Fe and more pronounced P inclusion in ExINP-ENA particle samples (especially ENA2020-18 and ENA2020-36) than ACE-ENA samples. While the source of observed discrepancies between the two studies is uncertain, we presume the use of different inlet and filter impactor systems (and resulting different sizes of collected particles) can act as the source besides different air mass sources. In fact, the K22 particle samples were collected using a micro orifice uniform deposit impactor with a 50% cut-size of 0.56 µm in aerodynamic diameter (Dae) whereas the particle sampling system employed for ExINP-ENA allowed the collection of particles up to 8 µm in Dae.

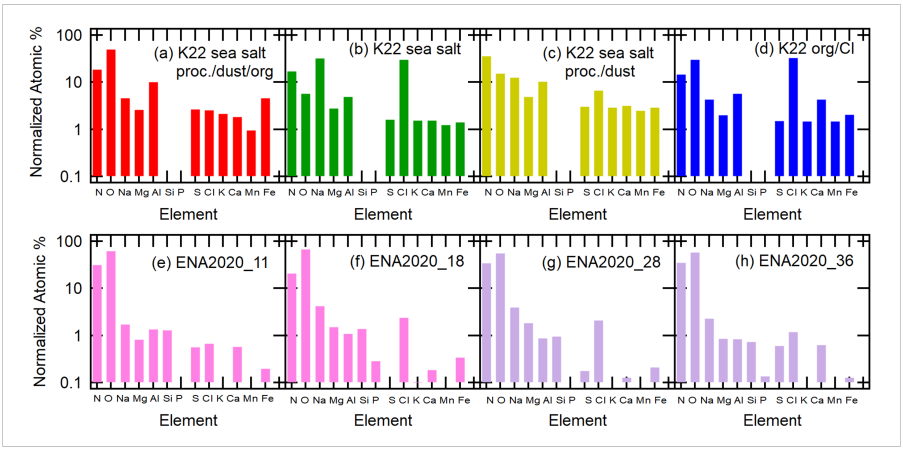

Figure S1. Figure S1. SEM-EDX-based particle elemental composition data from ACE-ENA 2017 (a-d) and ExINP-ENA 2020 (e-h)

Although it is apparent that the population of aerosols at ENA is unique from other marine sites, the physicochemical properties are not well understood and warrant much closer study. Characterization of the mixing state of particles should be examined to compare with other, better understood sites. Glassy aerosols may act as INPs, so the viscosity should also be studied (Berkemeier et al., 2014). Finally, as many of the best INPs are organics with biological origin, samples from ENA could be explored using both chemical characterization methods including mass spectrometry and biological characterization methods including proteomic and metabolomic methods to discover whether the biological aerosols (Huang et al., 2021) present at the site are undergoing processes distinct to this site. The differences between our study and (Knopf et al., 2022) can be attributed to many factors including, but not limited to, underestimation of sea spray INP concentrations in M18 (e.g., (Cornwell et al., 2021)), different air masses, and different inlet and filter impactor systems.

Text S6. Using Poisson statistics to determine temperature-dependent errors from online methods

The temperature uncertainty for PINE-measured INPs was estimated to be ±1.5°C (Hiranuma et al., 2022). This temperature uncertainty is mainly due to the inhomogeneity in the temperature readings at different locations inside the PINE chamber during the expansion run (Möhler et al., 2021). We measured the INP number concentrations of ambient and filtered air with the PINE instrument. Because INP concentrations vary with temperature, the errors associated with INPs are also temperature dependent. We estimate the temperature-

dependent errors in INP concentrations at four temperatures (−16 °C,−21 °C,−26 °C, and −31 °C). For closure analysis in the main text, we use errors obtained for −31 °C measurements to represent temperature-dependent errors in −29 °C INP measurements.

These errors were calculated from measurements of large particles detected during normal sampling procedures and those detected during times when the chamber was filled with filtered air (Krishnamoorthy & Lee, 2013). The filtered air represented the background INP concentrations, and the mean and error were calculated with Poisson statistics based on equations 6 and 8 from Krishnamoorthy and Lee (2013). The statistical validity of the calculated mean was ensured by comparison with the calculated Z statistic, which showed the statistical significance of data points above −16 °C. To ensure the calculated error is applicable to the entire dataset, background and ambient measurements were made on at least three separate days. The 95% CIs at −21 °C, −25 °C, and −31 °C were 1.56 ± 0.93, 6.05 ± 1.41, and 23.28 ± 3.81 L^{-1}, respectively.

Data Set S1. SEM-EDX

Filter name	Start date/time	End date/time	Sea salt percent	Dust percent	Na/CL ratio
ENA2020-11	10/11/20 14:24	10/14/20 15:30	29 ±21	68 ±14	2.73 ±0.20
ENA2020-18	10/17/20 15:24	10/20/20 14:24	70 ±16	30 ±16	1.94 ±0.08
ENA2020-28	11/1/20 13:47	11/4/20 16:03	85 ±13	15 ±18	1.91 ±0.06
ENA2020-36	11/15/20 16:42	11/18/20 13:24	56 ±16	42 ±16	2.00 ±0.09

Table S2. Four samples collected on polycarbonate filters were analyzed with SEM-EDX to determine the percentage of particles primarily composed of salt (Na and Mg) and the percentage of particles primarily composed of dust (Al, Si, and Ca). The Na to Cl ratio is also presented. All data points are average ± standard error, n = 100.

Text S7. EAMv1 model description

We use the U.S. DOE Energy Exascale Earth System Atmosphere Model version 1 (EAMv1) (Neale et al., 2010; Golaz et al., 2022) with the modal aerosol module with four log-normal modes (MAM4) (Wang et al., 2020) to simulate the size-resolved aerosol composition inputs for the INP parameterizations. Here, we use interstitial and cloud-borne aerosol simulated using the MAM4 prognoses. Sea spray aerosol emissions in MAM4 are based on Mårtensson et al. (2003) parameterization for particle diameters from 0.020 µm to 2.5 µm and Monahan et al. (1986) from 2.5 µm to 10 µm. Marine Organic Aerosol (MOAs) in sea spray are simulated by the Organic Compounds from Ecosystems to Aerosols: Natural Films and Interfaces via Langmuir Molecular Surfactants (OCEANFILMS) emission source function (Burrows et al., 2018, 2022). Dust emissions are simulated as a function of threshold surface wind friction velocity and soil type (Mahowald et al., 2006) and the size distribution of dust follows Zender et al. (2003). Detailed evaluations of MAM4 aerosol in EAMv1 are available in Wang et al. (2020).

Text S8. Immersion-mode INP parameterizations

To estimate sea spray INP concentrations, we use the McCluskey et al. (2018) $n_s(T)$ parameterization along with the total sea spray surface area (M18). For mineral dust, we select multiple $n_s(T)$ parameterization fits discussed in Boose et al. (2016) because of the substantial uncertainties in mineral dust ice nucleating abilities in the literature (e.g. Boose et

al., 2016; Atkinson et al., 2013; Kanji et al., 2017). Specifically, we select the $n_s(T)$ fits for Moroccan and Peloponnese dust samples that possess the highest and lowest ice nucleating abilities, respectively, as shown in Figure 5 of Boose et al. (2016). These sites are also closer to ENA (a few thousand kilometers). For representing the median $n_s(T)$ estimates, we select the Ullrich et al. (2017) parameterization (UL17) which was developed using the global dust samples in Aerosol Interaction and Dynamics in the Atmosphere (AIDA) chamber ice nucleation experiments. To account for the particle size dependence of INPs, we also use size-dependent $n_s(T)$ parameterizations for dust adopted from Reicher et al. (2019) (REI19 sub-micron and REI19 super-micron). We compare different $n_s(T)$ in Text S9.

Text S9. Ice Nucleation Active Site Densities at ENA

Ice-nucleation-active site density (INAS, $n_s(T)$) has been commonly used to quantify the ice nucleation efficiency of single minerals (e.g. McCluskey et al., 2019; Ullrich et al., 2017; Boose et al., 2016; Mitts et al., 2021). $n_s(T)$ represents the INP concentrations that are normalized by the dry aerosol surface area. Figure S2 compares several temperature dependent $n_s(T)$ parameterizations for dust and sea spray INPs. M18 $n_s(T)$ estimates for sea spray INPs (blue line, Figure S2) are lower by at least three orders of magnitude than most dust $n_s(T)$ curves, consistent with the previous findings that dust is more ice active than sea spray aerosols (DeMott et al., 2016).

On the other hand, dust $n_s(T)$ calculated using different parameterizations differ by several orders of magnitude, even though all represent the same INP category of dust. For example, at $-20°$C, dust $n_s(T)$ parameterizations range from $1.0 \times 10^8\,\mathrm{m}^{-2}$ to $1.0 \times 10^{11}\,\mathrm{m}^{-2}$. The $n_s(T)$ estimates for airborne dust samples (B16 Peloppenesse, REI) are generally lower than those for surface dust sediments (UL17) and milled samples (B16 Morocco), which implies that the atmospheric transformation during long-range transport affects the INP efficiency of dust, consistent with previous studies (Boose et al., 2016).

Text S10. Aerosol-INP closure Figure S2 illustrates a schematic outline of the INP error decomposition method we use in this study.

We use the metric Modified normalized bias (MNB) to calculate the closure error. MNB is symmetric, ranges between -2 (under prediction) and 2 (over prediction), and the normalization makes it less sensitive to outliers compared to other error metrics such as the root mean squared error. MNB values close to zero indicate the best agreement between the two

INP type	$n_s(T)$	**Aerosol property**	**Sample type and conditions**
Sea spray	M18 (McCluskey et al., 2018)	Sea spray aerosol surface area concentration (0.08 µm to 10 µm) [$m^{-2}\,m^{-3}$]	Background sea spray samples collected at Mace Head station in clean marine conditions.
Dust	B16 Peloponnese (Boose et al., 2016)	Dust aerosol surface area concentration (0.08 µm to 10 µm) [$m^{-2}\,m^{-3}$]	Airborne sample from a single dust event collected in Peloponnese; dominated by calcite.
Dust	B16 Morocco (Boose et al., 2016)	Dust aerosol surface area concentration (0.08 µm to 10 µm) [$m^{-2}\,m^{-3}$]	Surface sample collected in Morocco and milled for IN experiments; dominated by Quartz.
Dust	UL17 (Ullrich et al., 2017)	Dust aerosol surface area concentration (0.08 µm to 10 µm) [$m^{-2}\,m^{-3}$]	Ground samples of desert dust from different locations.
Dust	REI19 supermicron (Reicher et al., 2019)	Dust aerosol surface area concentration (1 µm to 10 µm) [$m^{-2}\,m^{-3}$]	Airborne dust particles collected during different dust events in the eastern Mediterranean.

Table S3. Immersion-mode INP parameterizations used in this study.

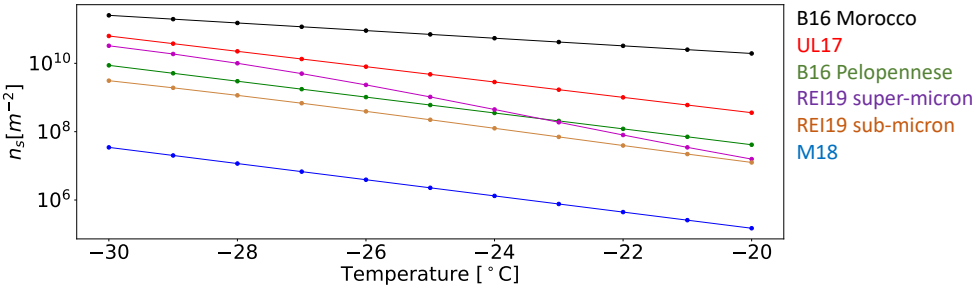

Figure S2. Ice active site density parameterizations for dust and sea spray populations plotted against freezing temperatures.

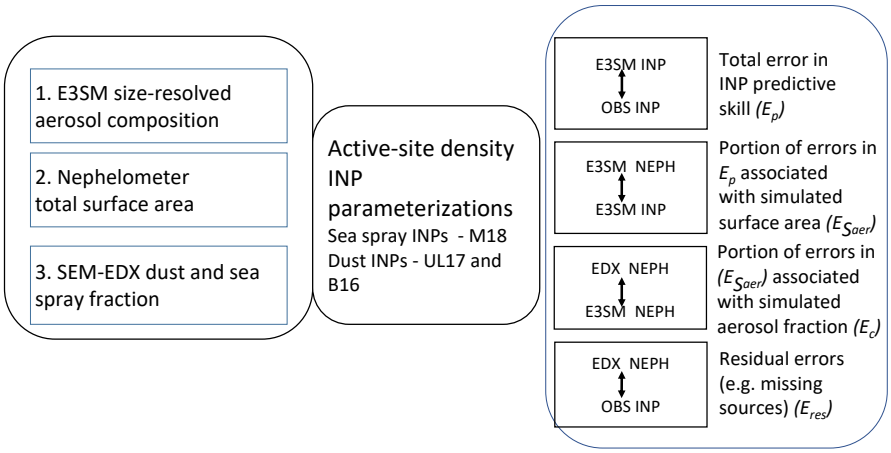

Figure S3. Schematic outline of the INP closure analysis

quantities. Eskes et al. (2015) used a similar metric called modified normalized mean bias (MNMB) to validate the predictability of atmospheric composition in the The Monitoring Atmospheric Composition and Climate (MACC) global analysis and forecast system. The difference between the metric MNB and MNMB is that MNMB is calculated as two times the average of MNB.

Text S11. Uncertainty propagation

We quantify the uncertainty in each error source given the independent aerosol and INP measurements. Here, we describe the uncertainty propagation technique to quantify uncertainties in the total INP discrepancy due to uncertainties in aerosol composition and residual sources. We define the uncertainty in E_c ($\partial \mathrm{E_c}$) due to uncertainties in SEM-EDX aerosol classification as:

Table S4. Closure error for the combined INPs from M18 and different dust INP parameterizations at different temperatures. INP concentrations are calculated using the observed aerosol fraction and total surface area from EDX and the nephelometer, respectively.

Temp	INP parameterization	Closure error temporal mean
$-29°C$	M18 + B16 Morocco	0.98
$-29°C$	M18 + UL17	0.89
$-29°C$	M18 + REI19 super	0.79
$-29°C$	M18 + B16 Pelopennese	0.45
$-27°C$	M18 + B16 Morocco	0.98
$-27°C$	M18 + UL17	0.89
$-27°C$	M18 + REI19 super	0.70
$-27°C$	M18 + B16 Pelopennese	0.39
$-25°C$	M18 + B16 Morocco	0.97
$-25°C$	M18 + UL17	0.70
$-25°C$	M18 + REI19 super	0.11
$-25°C$	M18 + B16 Pelopennese	-0.15
$-22°C$	M18 + B16 Morocco	0.94
$-22°C$	M18 + UL17	0.32
$-22°C$	M18 + REI19 super	-0.27
$-22°C$	M18 + B16 Pelopennese	-0.15

$$\delta \mathrm{E_c(T)} = \frac{\partial \mathrm{E_c(T)}}{\partial \mathrm{INP_{EDX\ NEPH}(T)}} \left(\frac{\partial \mathrm{INP_{EDX\ NEPH}(T)}}{\partial \mathrm{e_{du}}}\, \partial \mathrm{e_{du}} + \frac{\partial \mathrm{INP_{EDX\ NEPH}(T)}}{\partial \mathrm{e_{ss}}}\, \partial \mathrm{e_{ss}} \right)$$
$$= \frac{-2\ \overline{\mathrm{INP_{E3SM\ NEPH(T)}}}}{\left(\overline{\mathrm{INP_{E3SM\ NEPH(T)}}} + \overline{\mathrm{INP_{EDX\ NEPH(T)}}}\right)^2} \Big(\overline{n_{s(\mathrm{du})}(T) S_{\mathrm{aer(Neph)}} \delta e_{\mathrm{du}}}$$
$$+ \overline{n_{s(ss)}(T) S_{\mathrm{aer(Neph)}} \delta e_{\mathrm{ss}}} \Big), \quad (2)$$

where $\frac{\partial \mathrm{INP_{EDX\ NEPH}(T)}}{\partial \mathrm{e_{du}}}$ is the change in predicted INP concentrations using observed aerosol properties due to the uncertainties in dust fraction measured by SEM-EDX, $\partial \mathrm{INP_{EDX\ NEPH}(T)} \overline{\partial \mathrm{e_{ss}}}$ is the change in predicted INP concentrations using observed aerosol properties due to the uncertainties in sea spray fraction measured by SEM-EDX, $n_{s(\mathrm{du})}(T)$ and $n_{s(\mathrm{ss})}(T)$ denote the temperature-dependent ice-active site density parameterizations for dust and sea spray, respectively, $S_{\mathrm{aer(Neph)}}$ denotes the nephelometer-based total surface area, and e_{du} and e_{ss} denote the errors in EDX-derived dust and sea spray fractions, which can arise from various factors such as electron intensity stability, beam spot size accuracy, detected X-ray counting efficiency, and magnification or focus precision. We describe the notation and the INP calculations in Table **??**.

We define the uncertainty in E_{res} ($\partial \mathrm{E_{res}}$) due to temperature-dependent errors in PINE INP measurements (δ INP OBS) as:

$$\delta \mathrm{E_{res}} = \frac{\partial \mathrm{E_{res}}}{\partial \mathrm{INP_{INP\ OBS}}}\ \delta \mathrm{INP_{INP\ OBS}}$$
$$= \frac{-2\ \overline{\mathrm{INP_{EDX\ NEPH}}}(\mathrm{T})}{\left(\overline{\mathrm{INP_{EDX\ NEPH}}}(\mathrm{T}) + \overline{\mathrm{INP_{OBS}}}(\mathrm{T})\right)^2}\ \delta \mathrm{INP_{INP\ OBS}}, \quad (3)$$

Due to the sparse availability of SEM-EDX observations for the campaign time period, we use the mean INP concentrations of all SEM-EDX samples to estimate MNB for error sources E_c and E_{res}. For the other error components $E_{S_{aer}}$ and E_p, we estimate MNB using the 6-hourly averaged INP concentrations.

References

Atkinson, J. D., Murray, B. J., Woodhouse, M. T., Whale, T. F., Baustian, K. J., Carslaw, K. S., ... Malkin, T. L. (2013). The importance of feldspar for ice nucleation by mineral dust in mixed-phase clouds. *Nature*, *498*(7454), 355–358.

Berkemeier, T., Shiraiwa, M., Pöschl, U., & Koop, T. (2014). Competition between water uptake and ice nucleation by glassy organic aerosol particles. *Atmospheric Chemistry and Physics*, *14*(22), 12513–12531.

Boose, Y., Welti, A., Atkinson, J., Ramelli, F., Danielczok, A., Bingemer, H. G., ... Lohmann, U. (2016). Heterogeneous ice nucleation on dust particles sourced from nine deserts worldwide–part 1: Immersion freezing. *Atmospheric Chemistry and Physics*, *16*(23), 15075–15095.

Burrows, S. M., Easter, R., Liu, X., Ma, P.-L., Wang, H., Elliott, S. M., ... Rasch, P. J. (2018). Oceanfilms sea-spray organic aerosol emissions–part 1: implementation and impacts on clouds. *Atmospheric Chemistry and Physics Discussions*, 1–27.

Burrows, S. M., Easter, R. C., Liu, X., Ma, P.-L., Wang, H., Elliott, S. M., ... Rasch, P. J. (2022). Oceanfilms (organic compounds from ecosystems to aerosols: Natural films and interfaces via langmuir molecular surfactants) sea spray organic aerosol emissions–implementation in a global climate model and impacts on clouds. *Atmospheric Chemistry and Physics*, *22*(8), 5223–5251.

Cornwell, G. C., McCluskey, C. S., DeMott, P. J., Prather, K. A., & Burrows, S. M. (2021). Development of heterogeneous ice nucleation rate coefficient parameterizations from ambient measurements. *Geophysical Research Letters*, *48*(23), e2021GL095359.

DeMott, P. J., Hill, T. C., McCluskey, C. S., Prather, K. A., Collins, D. B., Sullivan, R. C., ... others (2016). Sea spray aerosol as a unique source of ice nucleating particles. *Proceedings of the National Academy of Sciences*, *113*(21), 5797–5803.

Eskes, H., Huijnen, V., Arola, A., Benedictow, A., Blechschmidt, A.-M., Botek, E., ... others (2015). Validation of reactive gases and aerosols in the macc global analysis and forecast system. *Geoscientific model development*, *8*(11), 3523–3543.

Golaz, J.-C., Van Roekel, L. P., Zheng, X., Roberts, A. F., Wolfe, J. D., Lin, W., ... others (2022). The doe e3sm model version 2: overview of the physical model and initial model evaluation. *Journal of Advances in Modeling Earth Systems*, *14*(12).

Hiranuma, N., Brooks, S. D., Moffet, R. C., Glen, A., Laskin, A., Gilles, M. K., ... McFarquhar, G. (2013). Chemical characterization of individual particles and residuals of cloud droplets and ice crystals collected on board research aircraft in the isdac 2008 study. *Journal of Geophysical Research: Atmospheres*, *118*(12), 6564–6579.

Hiranuma, N., Wilbourn, E. K., & Lacher, L. (2022). *Examining the ice-nucleating particles from the eastern north atlantic (exinp-ena) field campaign report* (Tech. Rep.). Oak

Ridge National Lab.(ORNL), Oak Ridge, TN (United States). Atmospheric ....

Huang, S., Hu, W., Chen, J., Wu, Z., Zhang, D., & Fu, P. (2021). Overview of biological ice nucleating particles in the atmosphere. *Environment International*, *146*, 106197.

Jeol. (last accessed, August 11 2022). Scanning electron microscope a to z: Basic knowledge for using the sem. In *Jeol*.

Kanji, Z. A., Ladino, L. A., Wex, H., Boose, Y., Burkert-Kohn, M., Cziczo, D. J., & Krämer, M. (2017). Overview of ice nucleating particles. *Meteorological Monographs*, *58*, 1–1.

Knopf, D. A., Charnawskas, J. C., Wang, P., Wong, B., Tomlin, J. M., Jankowski, K. A., ... others (2022). Micro-spectroscopic and freezing characterization of ice-nucleating particles collected in the marine boundary layer in the eastern north atlantic. *Atmospheric chemistry and physics*, *22*(8), 5377–5398.

Krishnamoorthy, K., & Lee, M. (2013). New approximate confidence intervals for the difference between two poisson means and comparison. *Journal of Statistical Computation and Simulation*, *83*(12), 2232–2243.

Logan, T., Xi, B., & Dong, X. (2014). Aerosol properties and their influences on marine boundary layer cloud condensation nuclei at the arm mobile facility over the azores. *Journal of Geophysical Research: Atmospheres*, *119*(8), 4859–4872.

Mahowald, N. M., Muhs, D. R., Levis, S., Rasch, P. J., Yoshioka, M., Zender, C. S., & Luo, C. (2006). Change in atmospheric mineral aerosols in response to climate: Last glacial period, preindustrial, modern, and doubled carbon dioxide climates. *Journal of Geophysical Research: Atmospheres*, *111*(D10).

Mårtensson, E., Nilsson, E., de Leeuw, G., Cohen, L., & Hansson, H.-C. (2003). Laboratory simulations and parameterization of the primary marine aerosol production. *Journal of Geophysical Research: Atmospheres*, *108*(D9).

McCluskey, C. S., DeMott, P. J., Ma, P.-L., & Burrows, S. M. (2019). Numerical representations of marine ice-nucleating particles in remote marine environments evaluated against observations. *Geophysical Research Letters*, *46*(13), 7838–7847.

McCluskey, C. S., Hill, T. C., Sultana, C. M., Laskina, O., Trueblood, J., Santander, M. V., ... others (2018). A mesocosm double feature: Insights into the chemical makeup of marine ice nucleating particles. *Journal of the Atmospheric Sciences*, *75*(7), 2405–2423.

Mitts, B. A., Wang, X., Lucero, D. D., Beall, C. M., Deane, G. B., DeMott, P. J., & Prather, K. A. (2021). Importance of supermicron ice nucleating particles in nascent sea spray.

Geophysical Research Letters, *48*(3), e2020GL089633.

Möhler, O., Adams, M., Lacher, L., Vogel, F., Nadolny, J., Ullrich, R., ... others (2021). The portable ice nucleation experiment (pine): a new online instrument for laboratory studies and automated long-term field observations of ice-nucleating particles. *Atmospheric Measurement Techniques*, *14*(2), 1143–1166.

Monahan, E., Spiel, D., & Davidson, K. (1986). A model of marine aerosol generation via whitecaps and wave disruption. *Oceanic whitecaps: And their role in air-sea exchange processes*, 167–174.

Neale, R. B., Chen, C.-C., Gettelman, A., Lauritzen, P. H., Park, S., Williamson, D. L., ... others (2010). Description of the ncar community atmosphere model (cam 5.0). *NCAR Tech. Note NCAR/TN-486+ STR*, *1*(1), 1–12.

Reicher, N., Budke, C., Eickhoff, L., Raveh-Rubin, S., Kaplan-Ashiri, I., Koop, T., & Rudich, Y. (2019). Size-dependent ice nucleation by airborne particles during dust events in the eastern mediterranean. *Atmospheric Chemistry and Physics*, *19*(17), 11143–11158.

Testa, B., Hill, T. C., Marsden, N. A., Barry, K. R., Hume, C. C., Bian, Q., ... others (2021). Ice nucleating particle connections to regional argentinian land surface emissions and weather during the cloud, aerosol, and complex terrain interactions experiment. *Journal of Geophysical Research: Atmospheres*, *126*(23), e2021JD035186.

Uin, J., Smith, S., & Springston, S. (2020). *Eastern north atlantic (ena) aerosol observing system (aos) instrument handbook* (Tech. Rep.). Oak Ridge National Lab.(ORNL), Oak Ridge, TN (US). Atmospheric Radiation ....

Ullrich, R., Hoose, C., Möhler, O., Niemand, M., Wagner, R., Höhler, K., ... Leisner, T. (2017). A new ice nucleation active site parameterization for desert dust and soot. *Journal of the Atmospheric Sciences*, *74*(3), 699–717.

Wang, H., Easter, R., Zhang, R., Ma, P.-L., Singh, B., Zhang, K., ... others (2020). Aerosols in the e3sm version 1: New developments and their impacts on radiative forcing. *Journal of Advances in Modeling Earth Systems*, *12*(1), e2019MS001851.

Zawadowicz, M. A., Suski, K., Liu, J., Pekour, M., Fast, J., Mei, F., ... others (2021). Aircraft measurements of aerosol and trace gas chemistry in the eastern north atlantic. *Atmospheric Chemistry and Physics*, *21*(10), 7983–8002.

Zender, C. S., Bian, H., & Newman, D. (2003). Mineral dust entrainment and deposition (dead) model: Description and 1990s dust climatology. *Journal of Geophysical*

Research: Atmospheres, *108*(D14).

Zhang, D., Wang, Z., & Liu, D. (2010). A global view of midlevel liquid-layer topped stratiform cloud distribution and phase partition from calipso and cloudsat measurements. *Journal of Geophysical Research: Atmospheres*, *115*(D4).

Zimmermann, F., Weinbruch, S., Schütz, L., Hofmann, H., Ebert, M., Kandler, K., & Worringen, A. (2008). Ice nucleation properties of the most abundant mineral dust phases. *Journal of Geophysical Research: Atmospheres*, *113*(D23).

Zolles, T., Burkart, J., Hausler, T., Pummer, B., Hitzenberger, R., & Grothe, H. (2015). Identification of ice nucleation active sites on feldspar dust particles. *The Journal of Physical Chemistry A*, *119*(11), 2692–2700.